Proceedings of the ASME 2010 3rd Joint US-European Fluids Engineering Summer Meeting and 8th International Conference on Nanochannels, Microchannels, and Minichannels
FEDSM-ICNMM2010
August 1-5, 2010, Montreal, Canada

FEDSM-ICNMM2010-30839

NUMERICAL SIMULATION OF THE FLOW FIELD IN A STATICALLY AND DYNAMICALLY ECCENTRIC ANNULAR SEAL WITH NON-CIRCULAR WHIRL ORBITS

Anand Vijaykumar
Texas A&M University
College Station, Texas, USA

Gerald Morrison
Texas A&M University
College Station, Texas, USA

ABSTRACT

The flow field in an annular seal is simulated for synchronous circular whirl orbits with 60Hz whirl frequency and a clearance/radius ratio of 0.0154 using the Fluent CFD code. Fluent's Moving Reference Frame model (MRF) is used to render the flow quasi-steady by making transformations to a rotating frame. The computed flow fields for velocity, pressure and shear stress measurements are compared with the experimental data of Winslow (1994), Thames (1992) and Cusano (2006). The CFD predictions are found to be in good agreement with the experimental results. The present CFD methodology can be extended to other whirl frequencies and clearances. The dynamic wall pressure distributions in an annular seal for non-circular whirl orbits was obtained using CFD. The simulations were performed using a time dependant solver utilizing Fluent's Dynamic Mesh model and User Defined Functions (UDFs). The wall pressure distributions obtained from the simulations are compared with data of Cusano (2006). The CFD simulations over predicted the pressure field when compared to experimental results however the general trends in pressure contours are similar. The flow field for varying rotor eccentricities are also studied by performing coordinate transformations and rendering the flow quasi-steady at set eccentricities using Fluent's MRF model. The computed velocity and pressure fields are compared with the time dependant solution obtained using Fluent's Dynamic Mesh model and UDFs for the same eccentricity. Good agreement in the velocity fields is obtained however the pressure fields require further investigation.

INTRODUCTION

Turbomachinery seals interface between rotating parts such as rotors, blade tips and stationary parts such as housings. Seals help isolate regions of different pressures and are non-contacting; resulting in leakage flow across the seal. Annular seals are leakage control devices minimizing secondary flow in turbomachines. Although the annular seals are geometrically similar to plain journal bearings, they show a different flow structure which may be dominated by turbulence and inertia effects.

A simple annular seal primarily consists of a smooth rotating shaft concentric with a stationary smooth cylinder. The whirl phenomena can be attributed to the destabilizing forces which cause the shaft to rotate eccentrically inside the housing, Chen and Jackson (1987). The destabilizing forces are caused by misalignments due to static or dynamic loading of shafts and high relative roughness due to small clearances.

The secondary flow through the seal is unwanted as it reduces the efficiency of the machine. Operating conditions unique to seals are large axial pressure gradients and small clearance to radius ratios. The flow is important to analyze since it affects the performance of the seal as well as the forces which act upon the rotor.

CFD simulations are performed using flow parameters from the experiments of Cusano (2006), Robic (1999), Winslow (1994) and Thames (1992) so that the ability of CFD simulations to directly represent various flow fields can be verified. CFD simulations can help provide a faster and cheaper estimate of the flow field for a wide variety of operating parameters and flow conditions compared to experimental investigations.

The impetus for the present study is two-fold. First is to test the accuracy of the CFD model and the physical models utilized to simulate these types of problems where coordinate transformations are made. Flow fields for various eccentricities can be estimated by rendering the flow quasi-steady. A similar

methodology can be used for similar types of flows in other types of Tubomachinery seals. As with most of the commercial codes the accuracy of the codes need to be validated with experimental data.

The flow field in an annular seal is highly turbulent and hence it is important to analyze the flow in order to determine the seal performance and forces acting on it. Extensive data is available on annular seals through experimental studies at the Turbomachinery Laboratory. But complexities with the current experimental setups make it difficult to obtain information for a wide range of operating and flow conditions. CFD provides an excellent alternative to determine flow fields and turbulence measurements for different operating conditions and flow fields.

The orbits for shaft speeds of 3600 rpm with varying whirl ratios revealed that the orbits at higher whirl ratios are more and more non-circular. It was impossible to measure the pressure data around the rotor instantaneously as the pressure measurements were taken at fixed azimuthal locations along the stator while rotor is rotating. Instantaneous and phase averaged wall pressure for annular seals with dynamic eccentricities and a whirl ratio of one were recorded by Winslow (1994) and for different whirl ratios at a given eccentricity by Cusano (2006). The current work focuses on obtaining the velocity and pressure fields distribution in an annular seal using CFD. The Fluent based CFD analysis was performed on data of Cusano (2006), Winslow (1994) and Thames (1992) to compare velocity and pressure fields.

NOMENCLATURE

c	Nominal clearance between rotor and stator (1.27 mm)
d	Rotor diameter
e	Rotor eccentricity ratio
ε	rotor eccentricity
L	Rotor length (37.3 mm)
P	Static pressure
P*m	(P-Pout)/(Pin-Pout)
R	Rotor radius (82.05 mm)
Re	Reynolds number = (2*U*c)/(ν)
Ta	Taylor number = (c*Wsh/ν)*(2c) $^{1/2}$/d
Ux	Mean axial velocity m/s
Um	Bulk averaged axial velocity, 7.4 m/s
Ur	Mean radial velocity m/s
Ut	Mean azimuthal velocity m/s
Wsh	Surface rotational speed of shaft.
μ	Dynamic viscosity
ν	Kinematic viscosity
ρ	Density of fluid
Cp	Sommerfeld Journal Bearing Coefficient
β	whirl ratio

NUMERICAL METHODOLOGY

The computations are performed using Fluent 6.3.26 which uses a control volume technique with a pressure based solver using segregated algorithms which solve the governing equations sequentially. The solution is iterated until a converged solution is obtained.

The present study utilizes the experimental work of Cusano (2006), Thames (1992), Winslow (1994), and Robic (1999) to compare with the CFD results. The 3D model is built using Gambit (Ver 2.4.6). The geometry of the model has the following dimensions- L =37.3mm, R =82.05mm and clearance= 1.27mm (50 mil). The rotor is maintained initially at an eccentricity of 50% (25mil). The 3D modeling is based on the actual seal geometry used in the experiments. The entire geometry is meshed using a hexahedral grid which consists of more than a million nodes. Fig. 1 shows the mesh and Fig. 2 show the grid independence study. The grid has high aspect ratio hexahedral cells as the variations along the tangential direction are small. In order to capture the flow conditions accurately near walls, the boundary layers along the rotor and stator walls must be resolved to y+ values of less than 5. The whirling motion of the rotor about the stator center was made possible using Fluent's Dynamic Mesh Model. The mesh is deformed every time step by treating the mesh as a series of interconnected springs. This is enabled using the '*rpsetvar*' command. The rotor is made to move along specific orbits paths by using User Defined Functions (UDF's) in Fluent, which are programs written in C programming language. Arbitrary orbit paths are represented by a polynomial equation. The rotor wall inside the meshed region was made to move along this orbit using UDFs in C language. Suitable transformations had to be made to ensure that orbit path makes an x intercept equivalent to 0.000635 m corresponding to the eccentricity of the rotor. Another UDF was written to print the centroid of the rotor after each timestep. The centroid coordinates were then compared with the curvefit equations to ensure that the rotor moves along specified orbit paths as it is not possible to observe the rotor motion in 3D due to complexity of grid and 3D rendering problems.

The Fig 1 shows the 3D mesh model which consists of 3 parts- swirl ring, the region between the rotor and the stator and the step region after the seal where the clearance increases. The swirl ring merely provides the inlet boundary condition for clearance and hence a relatively course mesh was used. The clearance region was meshed with a very fine mesh to ensure wall y+ values within specified limits. The space after the outlet is the region of larger clearance and is created long enough in order to prevent backflow from taking place at the outlet plane. The boundary condition for inlet plane is set as 'mass flow rate'. The mass flow rate was set to 4.87 kg/sec for a Reynolds number of 24000. The boundary conditions for turbulent parameters like turbulent kinetic energy and dissipation rate are set. The steady state simulation was performed first to provide an initial guess for the unsteady simulation. Unsteady simulations were performed once the steady solution converged. The good initial guess shortens the computational time. The unsteady simulations were performed at each time step until the residuals for x,y,z velocities, turbulent kinetic energy, turbulent viscosity and continuity went below 1e-04.

Fig 3 shows the geometry along with the dimensions of the test rig rotor. The working fluid used is water with density of 998.2 kg/m3 and dynamic viscosity of 0.00103 kg/m-s. A shaft speed of 3600 RPM corresponds to a Taylor number 6600. The inlet mass flow boundary condition was specified with a mass flow rate of 4.87 kg/s for a Reynolds number of 24,000. Standard k-ε models and wall-functions with pressure gradient effects were used to model the turbulence. The enhanced wall treatment is necessary to capture flow characteristics accurately in the viscous sublayer next to the wall. The standard wall function does not sufficiently resolve the viscous sublayer, and is not very effective when the wall is moving rapidly or when there are high pressure gradient effects. Ideally the wall y+ values should be below 1 but Fluent allows wall y+ values as large 5 as long as the first layer of the mesh lies in the viscous sublayer. The wall y+ value is equal to or below 5 throughout the seal except for the entrance region. Fig 4 shows the wall y+ distribution obtained in this study. Fig 7 shows the flow chart for dynamic mesh scheme. The coordinate transformations were performed using Fluent's Moving Reference Frames model (MRF) which renders the flow field quasi steady thereby enabling steady state simulations.

RESULTS

Circular Orbit, 50%Eccentricity, And 60Hz Whirl

For this flow case the flow rate is 4.87 l/s with 60Hz whirl frequency and a rotor rpm of 3600 (Wsh= -30.9 m/s). The Reynolds number is 24000, the Taylor number is 6600 and the eccentricity is 50%. The path of flow of fluid in the seal is show in Fig 6. The plenum ensures uniform flow into the seal and ensures there is no debris in the flow. The plenum was followed by a swirl ring to produce an inlet swirl for the flow entering the seal. The swirl angle was increased by placing an annular diffuser after swirl blades which slows the axial velocity at the same time increasing the swirl angle. There were no swirl blades installed for these simulations. The flow experiences a slight step at the inlet of the seal owing to difference in clearances from the exit of the diffuser to the inlet of the seal. The step has a considerable effect on the flow field in the seal.

The Fig 8.a-c, 9.a-c, 10.a-c, 11.a-c, 12.a-c, 13.a-c show the axial, radial tangential velocity fields at the seal inlet plane and at a location 85% downstream of the seal entrance. The experimental data are from Thames (1992). Also included in each figure are the results from the two different CFD techniques used to simulate the whirl ratio 1, 50% eccentric ratio, circular orbit seal results. The axial velocity near the inlet shows an accelerating flow near the pressure side with low velocities on the suction side. Fig 5 defines the pressure and suction side locations. As the flow progresses further downstream, the largest velocity magnitude region shifts from the pressure side towards the suction side. The highest velocity drops slightly half way down and increases again towards the exit of the seal. The numerical simulation results are in good agreement with the experimental results, however the numerical simulation results show a much thicker boundary layer compared to experimental results.

As the flow moves downstream, the peak axial momentum which was located at the inlet of the seal reaches wider clearances causing a slight decrease in the axial velocity. The axial velocity profile is more evenly distributed through out the seal. The radial velocities decrease as the flow is being directed down the seal and remain more or less constant. The radial velocities at the upstream and downstream positions are low throughout the seal. With the decrease in axial momentum, the tangential velocities increase. As the maximum axial velocity rotates around the seal the towards the suction side, the tangential velocities continue to increase towards the pressure side. Fig 14. a-b, Fig 15. a-b shows the axial and tangential velocity fields at Z/L = 0, 0.22, 0.49, 0.86 and 0.99 locations for UDF mesh motion and coordinate transform (MRF) cases.

The CFD azimuthal velocities at the seal inlet compare well to the experimental data. The small band of high axial velocity at the rotor surface is about the same for the both the experimental case and the Fluent simulations. Further downstream from inlet, the location of maximum axial velocity is convected around the seal accompanied by an increase in the tangential velocity component. There is good agreement between the experimental data with the Fluent simulations. However, the UDF mesh motion case predicts larger bands of high tangential velocity compared to the coordinate transformation case.

The tangential velocities at the inlet region show areas of low velocities. The Fluent UDF mesh motion case compares well with the experimental data however the coordinate transformed case predicts a larger region of low velocity. Both the Fluent simulations predict the small band of high tangential velocity at the high side along the rotor surface.

The coefficient of pressure plots for the UDF mesh motion case and the coordinate transformed case are presented in Fig 16.a-b. The high Cp and low Cp regions appear at the same locations at the seal entrance. However, there is a slight shift in regions of high Cp for the Moving Reference Case which is more in agreement with measurements by Winslow (1994).

50% Circular Orbit Statically Eccentric Case

For this flow case, the flow rate is 4.87 l/s with zero whirl ratio and a rotor rpm of 3600 (Wsh = -30.9 m/s). The Reynolds number is 24000, the Taylor number is 6600 and eccentricity ratio is 50%. The eccentric annular seal geometry exhibits a pressure distribution very similar to a journal bearing. As the rotor is eccentric about the stator center, the spinning of the rotor creates a pressure distribution which is very similar to the pressure and suction sides of a journal bearing. The region of constricting clearance position is called the pressure side and the suction side corresponds to expanding clearance position (Relative to positive θ direction). The largest and smallest clearance positions are called the high side and low side respectively. The different seal positions are show in Fig 5. Contours of non-dimensionalized axial (Ux/Um) and

azimuthal velocity (Ut/Um) are presented for the Maximum Clearance position, Minimum Clearance position, Pressure side and Suction side in Fig 17.a-c., 18.a-c., 19.a-c., 20.a-c., 21.a-c., 22.a.c., 23.a.c., 24.a.c. and compared with LDV measurements by Johnson (1989) and Shresta (1993). The axial velocities are the largest at the high and suction side at the inlet and largest at the pressure side at the exit of the seal. The axial flow characteristics can be explained based on journal bearing pressure field. As the flow enters the seal it gets pushed towards the high side and region of low pressure field which constitutes the suction side. Hence axial velocities are higher on the suction side when compared to the pressure side. As the flow moves downstream it gets pulled towards the pressure side owing to the wall shear stress of the spinning rotor. The spinning causes the axial momentum to be built up and move towards the pressure side.

The experimental results from LDA data have been non-dimensionalized using the average leakage velocity of 7.32 m/s. The results of Fluent 6.3.26 simulations for the static reference frame have been compared with the results from the coordinate transformed frame. The azimuthal velocity are higher on the low side compared to the high side and larger on the suction side compared to pressure side.

Mean Pressure And Mean Shear Stress For Circular Orbit 50% Eccentricity Case

For this flow case the flow rate is 4.87 l/s with a 60Hz whirl frequency with a rotor rpm of 3600 (Wsh = -30.9 m/s). The Reynolds number is 24000, the Taylor number is 6600 and the eccentricity ratio is 50%. The results for the pressure drop compare well with data obtained by Winslow (1994) as seen in Fig 25.a-b. Upstream of the seal inlet, the mean shear is low and the pressure is high. However, as the flow enters the seal they increase gradually due to restriction in the flow which occurs as the flow enters from a region of larger clearance to a smaller gap. A large pressure drop, Fig 25. a-b, occurs as the flow moves past the inlet region into the annulus. This has been found to be proportional to the eccentricity. The mean pressure recovers slightly past the inlet region owing to a 'vena contracta effect' which causes a small recirculation zone on the rotor surface. The experimental results show a steeper pressure drop as compared to numerical simulations. As the flow moves downstream, the pressure decreases linearly with axial direction. This can be attributed to frictional losses occuring in the seal.

The mean shear stress, Fig 25. c-d, is strongly effected by axial and azimuthal velocity gradients in the radial direction at the walls. The mean shear stresses are low at the inlet of the seal, however they increase as the fluid flows past the inlet. They remain fairly constant along the interior of the seal until at the exit where it rises rapidly. The Fluent simulations underpredict the mean shear stress measurements and show a more uniform profile, unlike the experimental data which has a fluctuating profile. The initial drop in mean shear stress downstream of the inlet can be attributed to the developing boundary layer which fully spans the clearance past Z/L = 0.2.

Non-Circular Whirl Orbits At 18Hz And 24Hz Whirl

For this flow case the flow rate is 4.87 l/s with 18Hz and 24Hz whirl frequencies (whirl ratios, β, of 0.3 and 0.4) with the rotor spinning at an rpm of 3600 (Wsh = -30.9 m/s). The Reynolds number is 24000, the Taylor number is 6600 and the whirl orbits are non-circular with varying eccentricity ratios. The simulations were performed for whirl ratios of 0.3and 0.4.

Contours of coefficient of pressure distributions (Fig 26) are presented for experimental (Cusano (2006)) and simulation results. C_p is derived as a variation of Sommerfield number. The axes presented show % cycle and Z/L which represent percentage cycle and normalized downstream position in the annular seal.

Fig 26.a-b shows the contour plots of the coefficient of pressure Cp for a whirl frequency of 18Hz (β=0.3). The experimental results indicate that at the inlet the minimum pressure is located at 20% of the cycle and the maximum pressure at 70%. However, as the flow progresses through the seal, the low and high pressure regions exchange positions with the maximum pressure occurring at 20% and the minimum at 70% at the seal exit. This same exchange was documented by Winslow (1994) for the same seal with a whirl ratio of 1. The Cp values for the 24Hz whirl frequency are presented in Fig 26.c-d. The exchange is not as obvious with the contours from the exit plane extending and decreasing in amplitude in the upstream direction. The magnitude of Cp is larger for the higher whirl ratio. For both whirl ratios, the Fluent UDF motion based simulations (time dependent simulations of the varying orbit path) over predicted the Cp values compared to experminental results by Cusano (2006). The Fluent Simulations exhibit regions of high and low Cp which present opposite trends at the downstream and upstream postions. Further investigation into the differences between the experimental data and the CFD simulations is necessary.

The time dependent, UDF motion based computer simulations are very computer resource intensive. In an effort to determine if a more efficient simulation approach is viable, an assumption of quasi-steady state was made. This assumption is similar to using the quasi-Couette flow assumption to represent the flow inside a tilt pad bearing. The current goal was to determine if the flow field present in a circular orbit flow case, which can be represented as a steady state calculation using the coordinate transform technique, can accurately represent the flow present with a varying orbit seal when the eccentricity ratios of both are the same. This would allow the simulation of a set number of steady state, circular orbit eccentricity ratios which would then be used to represent the flow whenever the non-circular orbit has the same instantaneous eccentric ratio. Fig 27. a-c, presents the static pressure contours for the coordinate transformation case and the UDF mesh motion case. Two UDF mesh motion results are presented. Both have the same eccentric ratio as the coordinate transform case but one was obtained from non-circular orbit with the same eccentricity ratio, as the eccentricity was increasing and the other while the eccentricity was decreasing. The results show that the shape of the pressure contours is the

same for all three cases. The two UDF mesh motion simulations are almost identical with respect to contour shape and pressure variation magnitude. This provides credence that the flow can be represented by a quasi-steady state assumption. The use of the coordinate transform steady state solution to provide this quasi-steady state solution is questionable. The contour shapes are very similar but the pressure levels are significantly different; a variation of 50 kPa for the coordinate transform case compared to 125 kPa for the UDF mesh motion. This factor of 2.5 times difference is unacceptable. Additional analysis is required to resolve the issue.

The flow field predicted for the three cases presented in Fig 27 are presented in Fig 28 and 29. Radial-azimuthal planes are presented at a location 15mm into the seal. Fig 28 illustrates that the magnitudes of the axial velocity are similar for all three cases. The region of maximum axial velocity for the two UDF cases brackets the location for the coordinate transform case. This indicates that even though the pressure distributions did not show memory of the previous seal eccentricity, the axial velocity does. Fig 29 shows the results for the azimuthal velocity component. All three cases are essentially identical.

CONCLUSIONS

3D CFD simulations of a whirling smooth annular seal are performed. Flow field comparisons are made between Fluent‘s Dynamic Mesh model which used a time dependant solver and Fluent’s Moving Reference Frame model which renders the flow quasi-steady. The flow field in the transformed frame show a good agreement with experimental results for statically eccentric case and circular orbit. The axial pressure distributions and the mean shear stresses matched experimental data for Fluent simulations in static frame as well as the transformed frame. However the contours of Cp show slight variations between the coordinate transformed frame case and the UDF mesh motion case.

The phase averaged wall pressure distributions aid in understanding the complex fluid processes occurring within the seal. The simulations were performed under zero pre-swirl conditions.

The general trends for 18Hz and 24Hz non-circular whirl orbits look similar however the Fluent simulations over predict the magnitude of the wall pressure distributions. Also the trends appear a little offset, this could be attributed to different whirl orbits recorded by Cusano (2006) for the same whirl frequency. The Fluent simulations simulate an averaged orbit of all the experimental orbits recorded by the probes at each downstream position.

A good estimate of the flow field and pressure distribution in an annular seal for different eccentricities can be made by statically setting the rotor at that eccentricity and using Fluent’s Moving Reference Frame model to compute the flow field in the transformed frame using a steady solver.

Future work needs to be done in order to refine CFD techniques for more accurate predictions. The grid refinement, wall functions and turbulence models used need further investigation.

REFERENCES

[1] Winslow, R.W., 1994, “Dynamic Pressure and Shear Stress Measurements on the Stator Wall of Whirling Annular Seals,” M.S Thesis, Texas A&M University, College Station.

[2] Thames, H.D., 1992, “Mean Flow and Turbulence Characteritics in Whirling Annular Seal,” M.S. Thesis, Texas A&M University, College Station.

[3] Cusano, D., 2006 “Experimental Phase-Averaged Wall Pressure Distributions for a 25% Eccentric Whirling Annular Seal” M.S. Thesis, Texas A&M University, College Station.

[4] Chen, W.C., Jackson, E.D., 1985 “Eccentricity and Misalignment Effects on the Performance of High-Pressure Annular Seals,” ASLE transactions, Vol. 28, pp. 104-110.

[5] Robic, B.F., 1999, “Experimental and Numerical Analysis of the Effect of Swirl on the Pressure Field in Whirling Annular and Labyrinth Seals,” Ph.D. Dissertation, Texas A&M University, College Station.

[6] Johnson, M.C., 1989, “Development of a 3-D Laser Doppler Anemometry System: With Measurements in Annular and Labyrinth Seals,” Ph.D. Dissertation, Texas A&M University, College Station.

[7] Shresta, S., 1993, “The Effects of Pre-swirl on Flow Through Centered and Eccentric Annular Seals,” M.S. Thesis, Texas A&M University, College Station.

[8] Das, P.G., 1993, “3-D Laser Doppler Velocimetry Measurements of Eccentric Annular and Labyrinth Seals,” M.S. Thesis, Texas A&M University, College Station.

[9] Arghir, M and Frene, J. July 1997b, “Analysis of a Test Case for Annular Seal Flows,” Transactions of the ASME, 119, pp. 408-414

[10] Morrison, G.L., Johnson, M.C., Tatterson, G.B., 1991 “Three-Dimensional Laser Anemometry Measurements in an Annular Seal,” Journal of Tribology, Vol. 113

[11] Athavale, M.M, Hendricks, R.C, Steinetz, B.M, 1995, “Numerical Simulation of Flow in a Whirling Annular Seal and Comparison With Experiments”, 31st Joint Propulsion Conference and Exhibit, San Diego, California.

[12] Athavale, M.M, Hendricks, R.C., 1996 “A Small Perturbation CFD Method for Calculation of Seal Rotordynamic Coefficients”, International Journal of Rotating Machinery, Vol. 2, pp. 167-177

[13] Suryanarayanan, A., 2003, “Experimental Measurement And Analysis of Wall Pressure Distribution for a 50% Eccentric Whirling Annular Seal,” M.S. Thesis, Texas A&M University, College Station.

[14] Park, S.H., 2006, “How to prepare the 3-D Mesh with whirling rotor using deforming mesh”, Tutorial, Texas A&M University, College Station.

[15] Sekaran, Aarthi., 2009, “Study of impact of orbit path, whirl ratio and clearance on the flow field and rotordynamic coefficients for a smooth annular seal”, M.S. Thesis, Texas A&M University, College Station.

APPENDIX

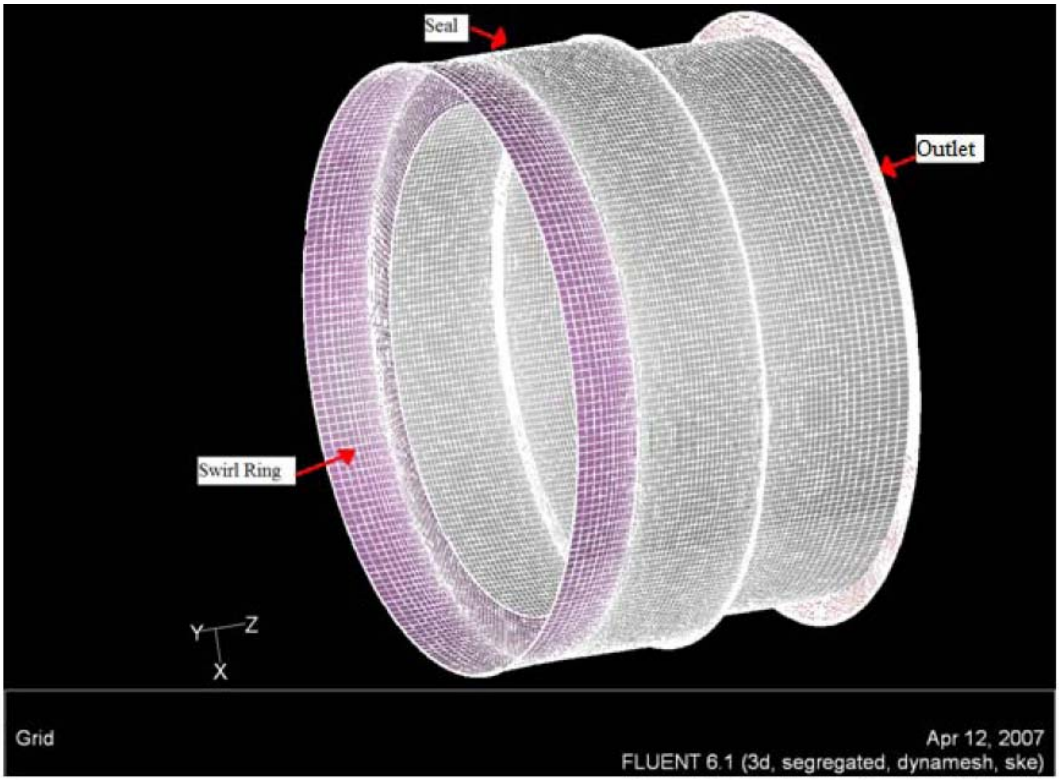

Fig. 1-Meshed Seal Geometry (from ref. 14)

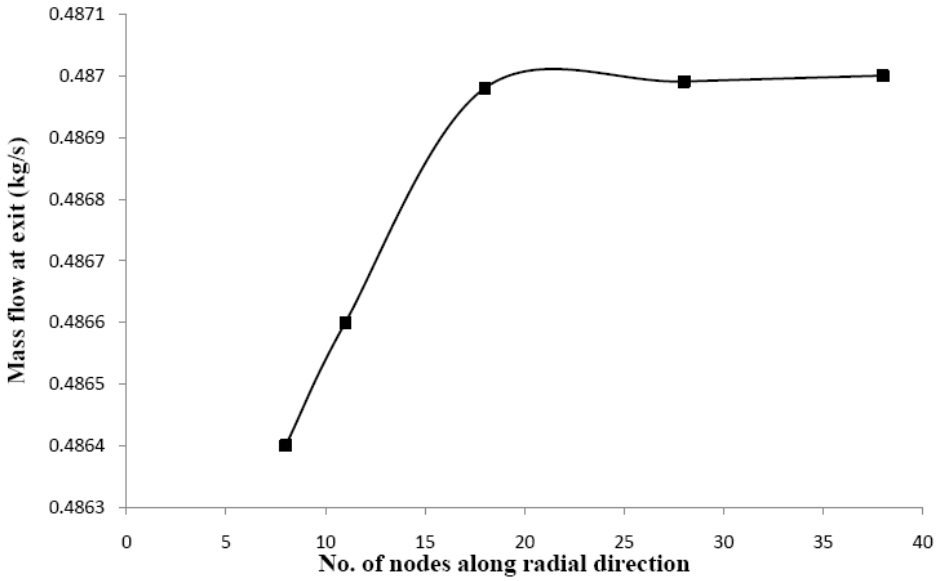

Fig. 2- Grid independence study (from ref. 14)

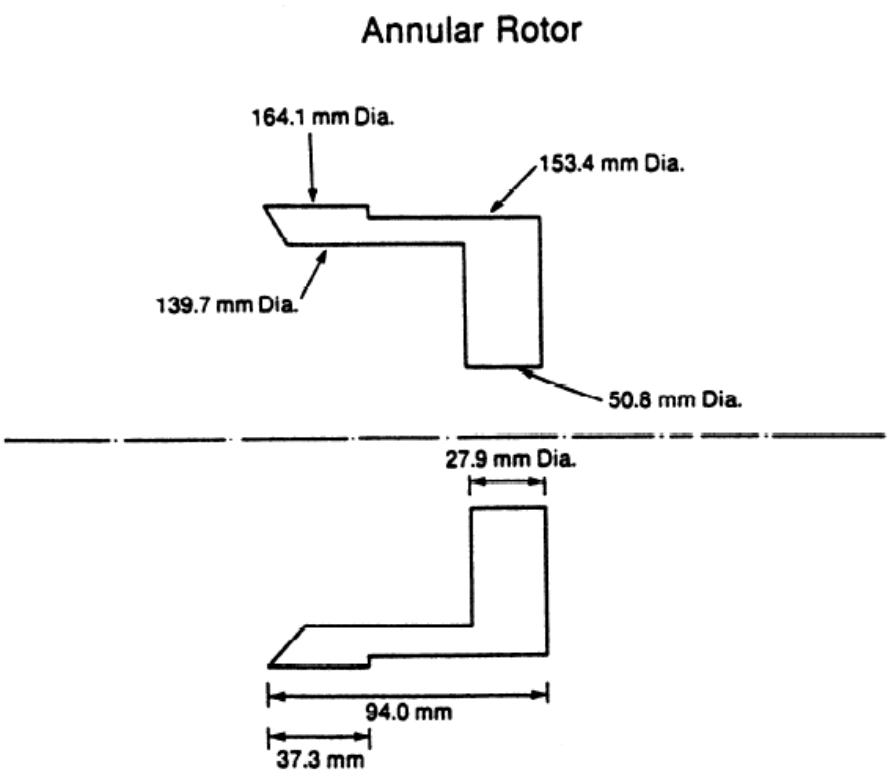

Fig. 3- test setup with dimensions (from ref. 6)

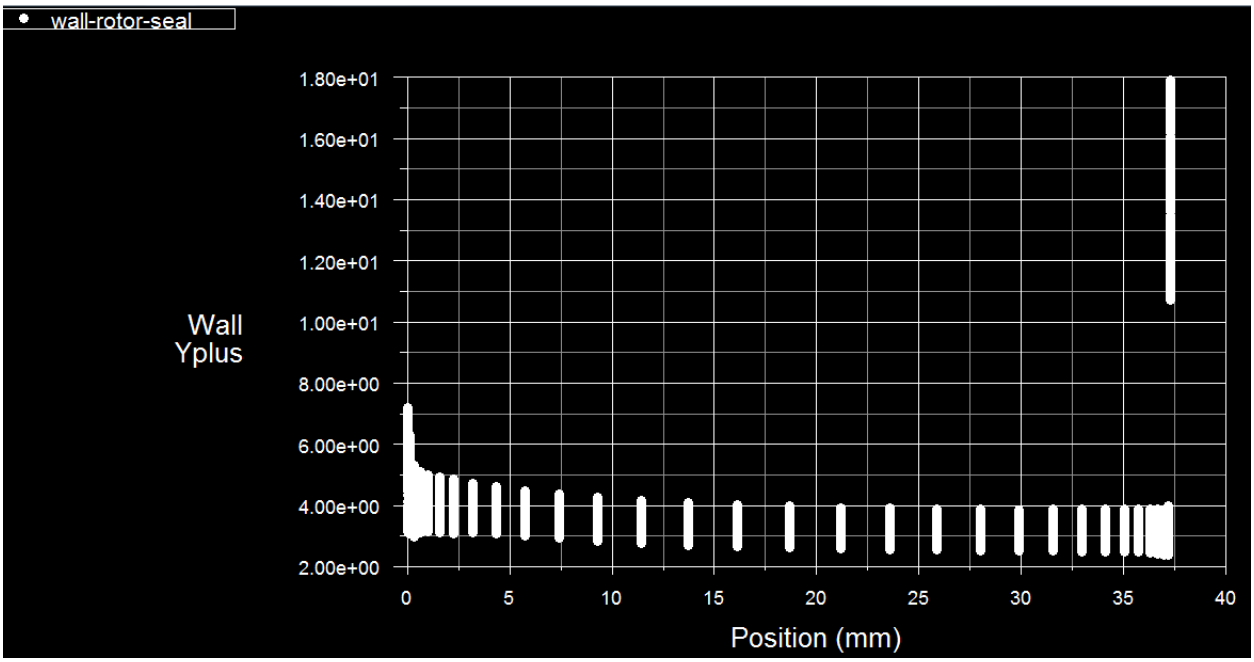

Fig. 4- XY plot of Wall Yplus Vs Position of seal

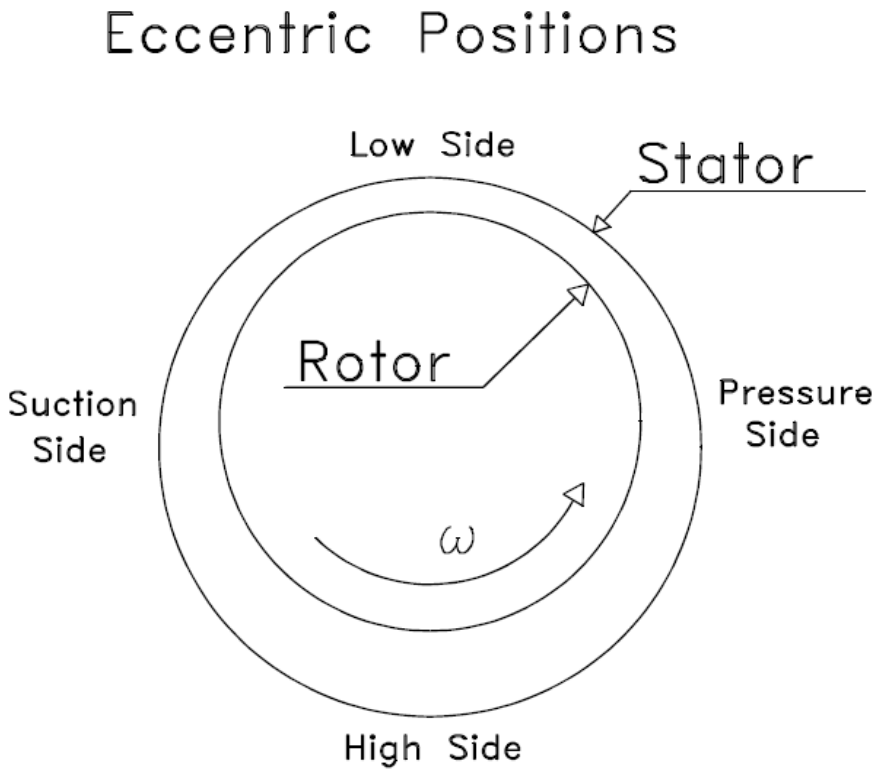

Fig. 5- Seal positions (from ref. 7)

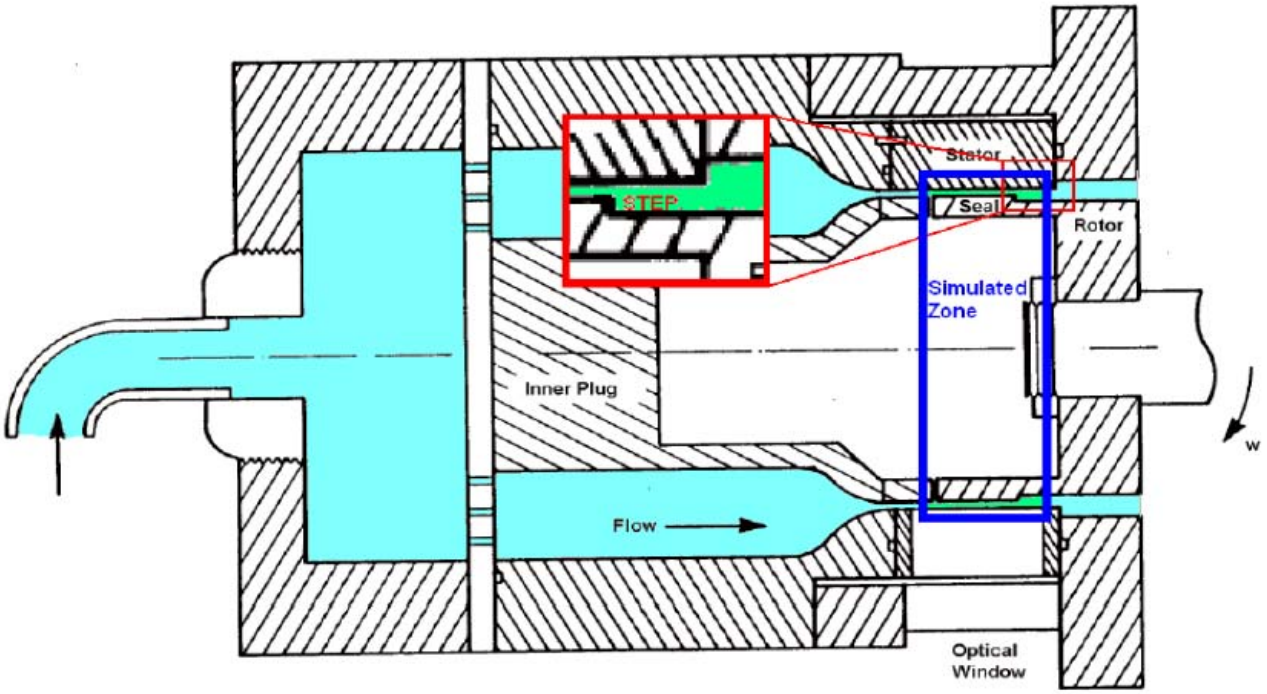

Fig. 6-Path of fluid in seal (from ref. 3)

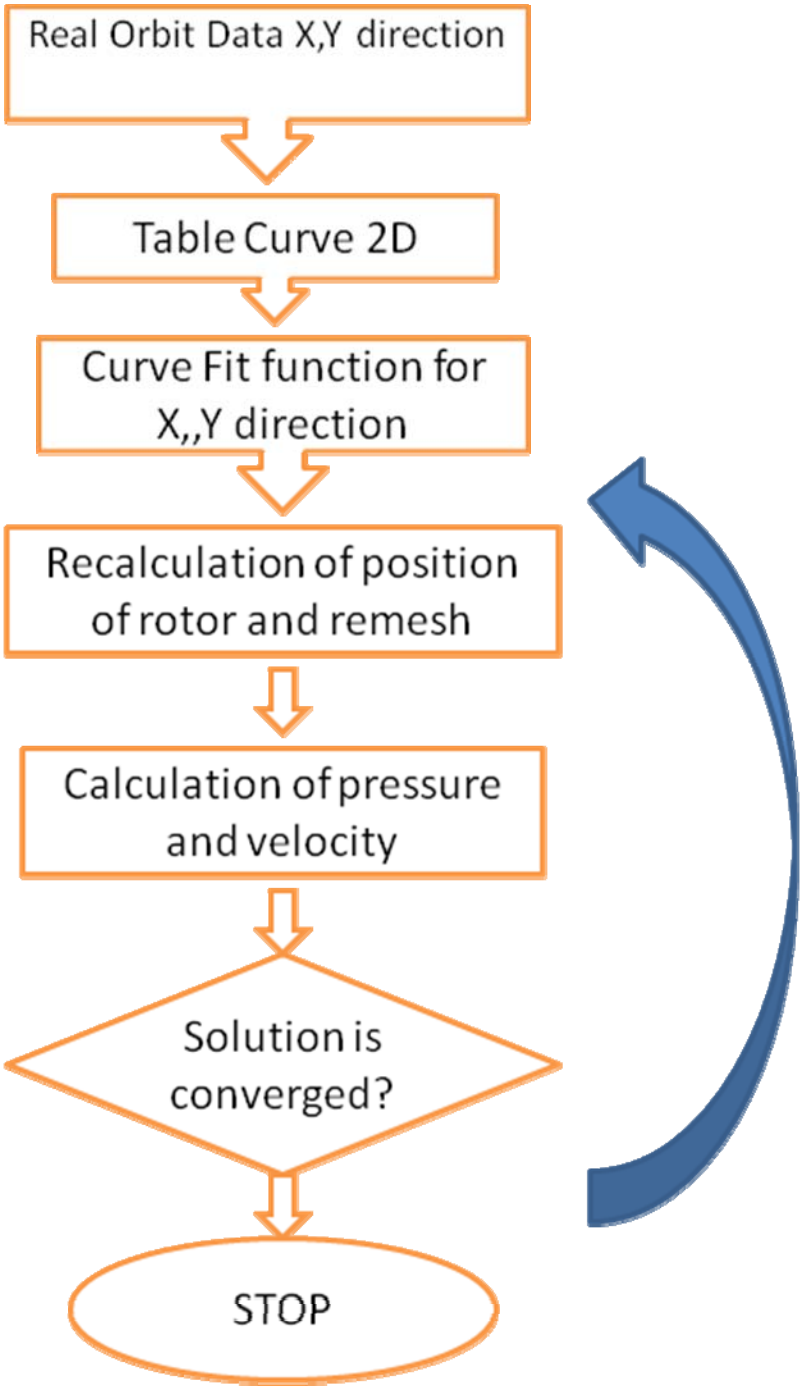

Fig. 7-Flowchart of dynamic mesh scheme

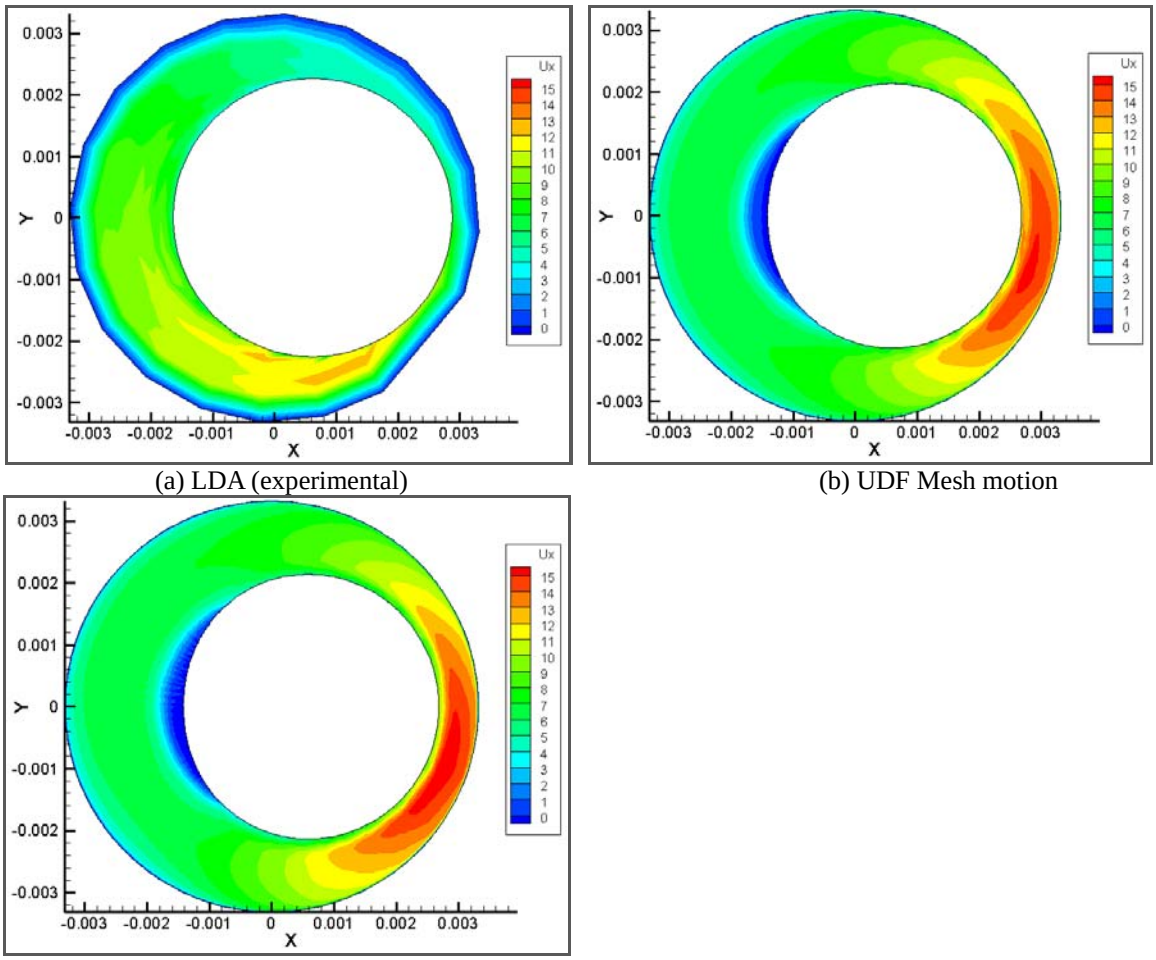

(a) LDA (experimental)

(b) UDF Mesh motion

(c) Coordinate Transform (MRF)

Fig. 8- contours of Ux at Z/L = 0. Seal whirl and spin in counterclockwise direction, clearances have been exagerrated for clarity.

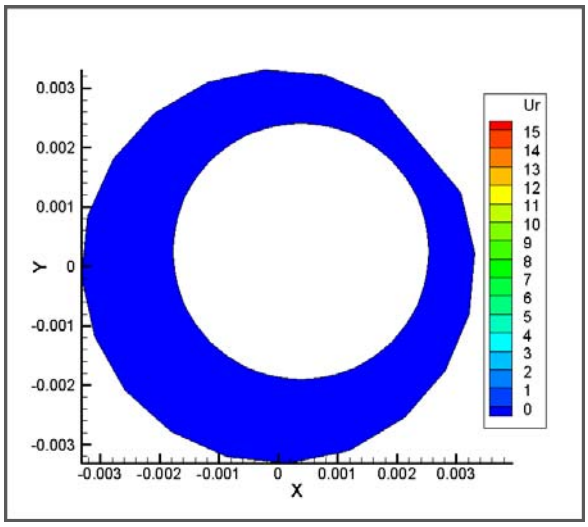

(a) LDA (experimental)

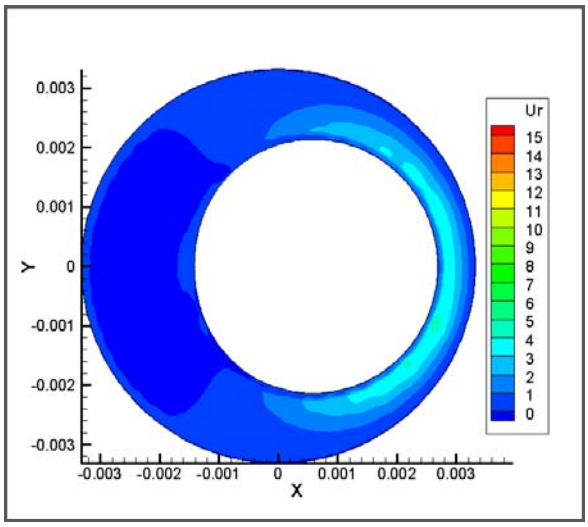

(b) UDF Mesh motion

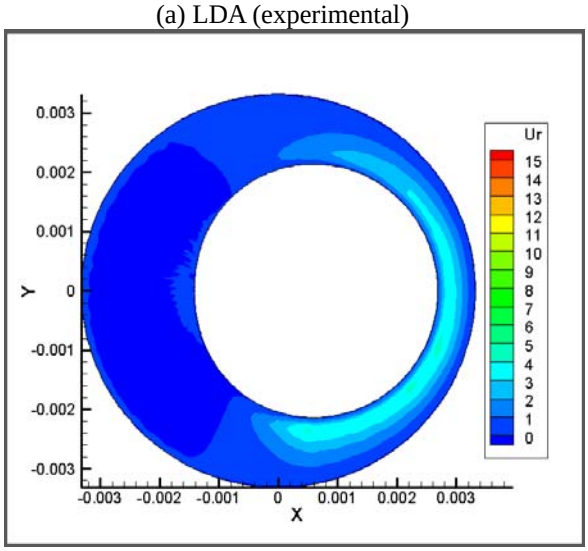

(c) Coordinate Transform (MRF)

Fig. 9- contours of Ur at Z/L = 0. Seal whirl and spin in counterclockwise direction, clearances have been exagerrated for clarity.

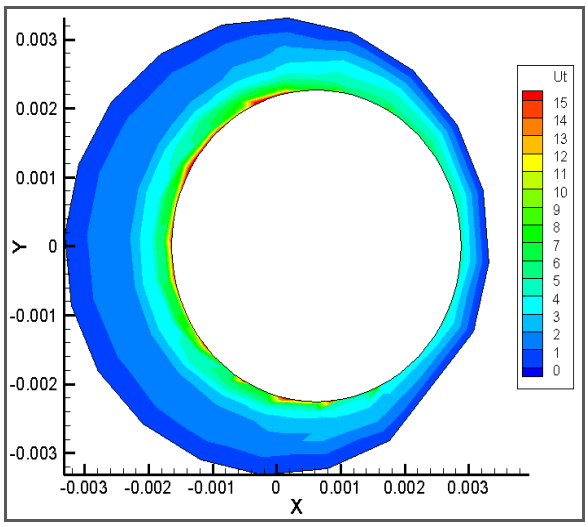

(a) LDA (experimental)

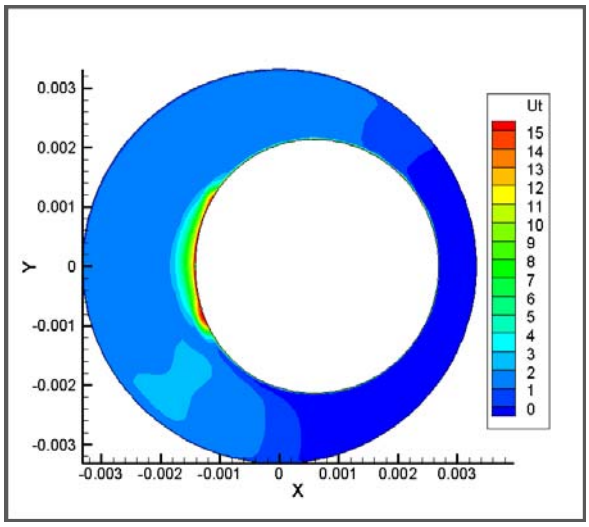

(b) UDF Mesh motion

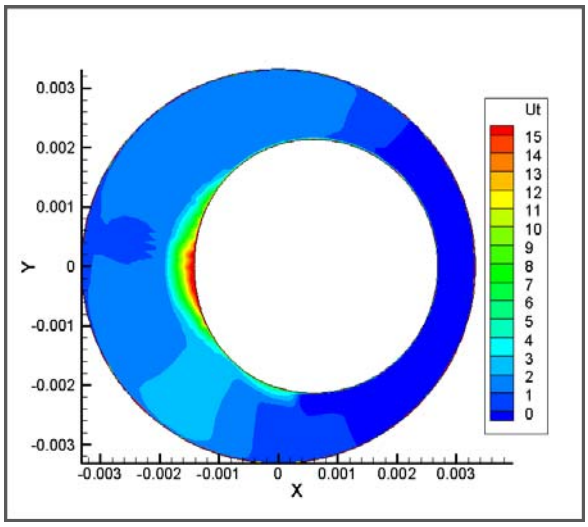

(c) Coordinate Transform (MRF)

Fig. 10- contours of Ut at Z/L = 0. Seal whirl and spin in counterclockwise direction, clearances have been exagerrated for clarity.

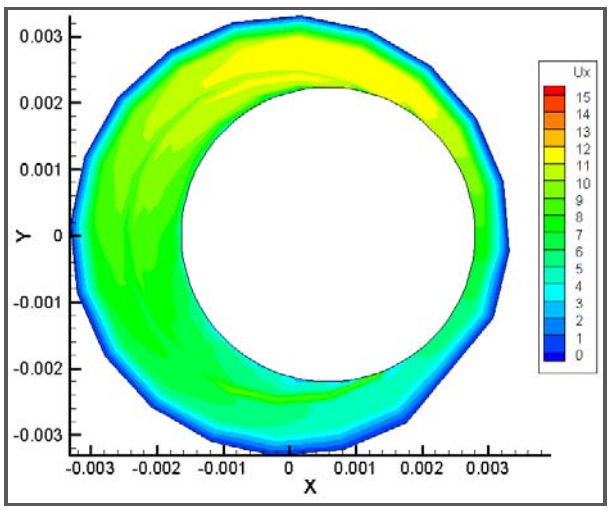

(a) LDA (experimental)

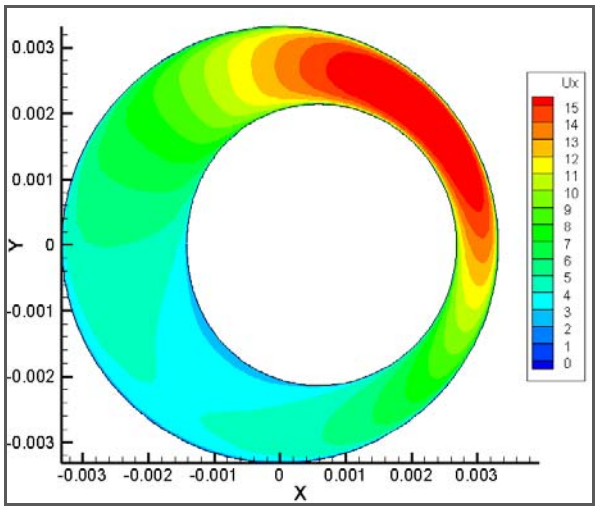

(b) UDF Mesh motion

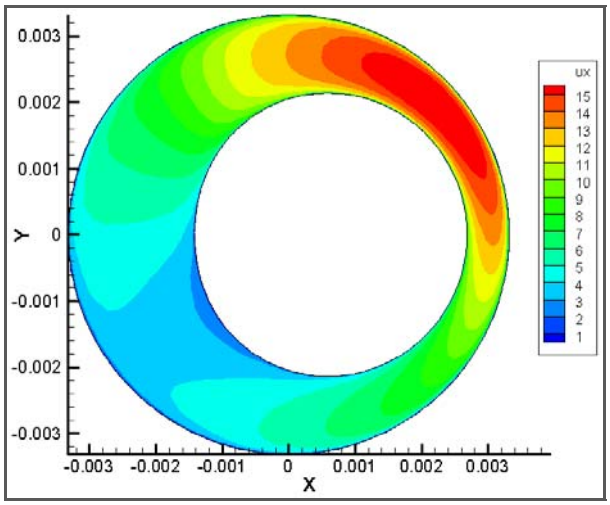

(c) Coordinate Transform (MRF)

Fig. 11- contours of Ux at Z/L = 0.850. Seal whirl and spin in counterclockwise direction, clearances have been exagerrated for clarity.

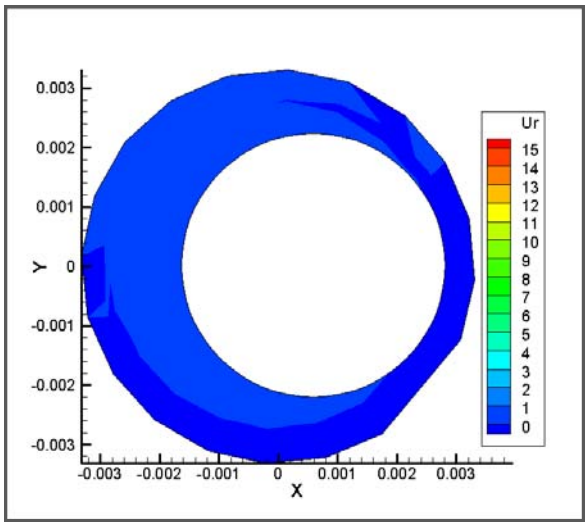

(a) LDA (experimental)

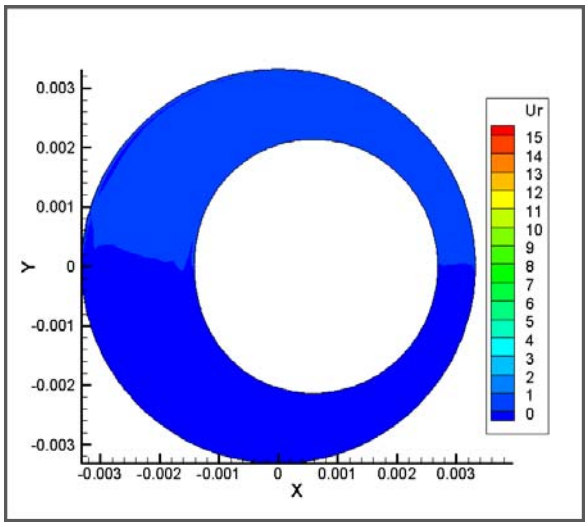

(b) UDF Mesh motion

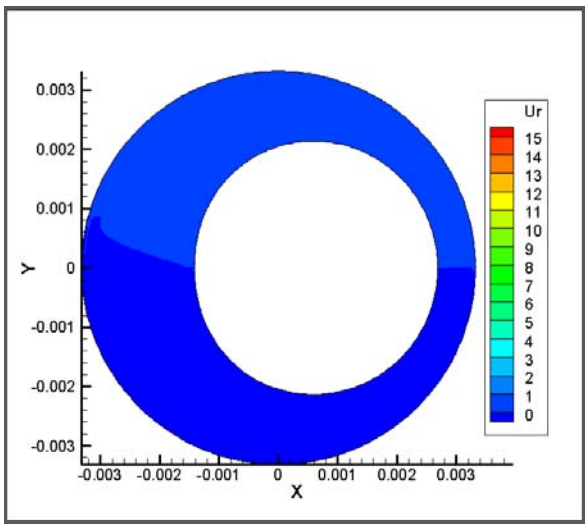

(c) Coordinate Transform (MRF)

Fig. 12- contours of Ur at Z/L = 0.850. Seal whirl and spin in counterclockwise direction, clearances have been exagerrated for clarity.

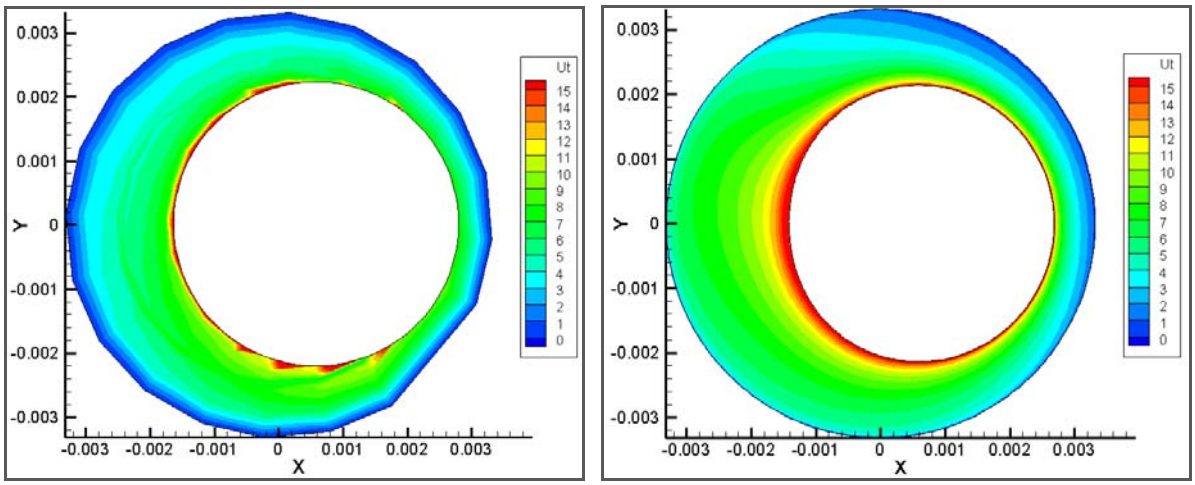

(a) LDA (experimental) (b) UDF Mesh motion

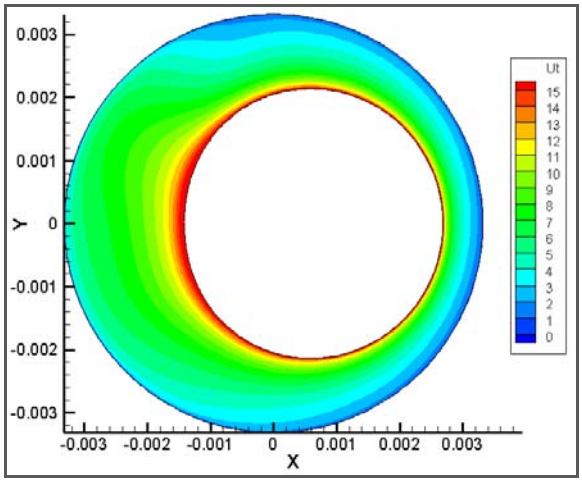

(c) Coordinate Transform (MRF)

Fig. 13- contours of Ut at Z/L = 0.850. Seal whirl and spin in counterclockwise direction, clearances have been exagerrated for clarity.

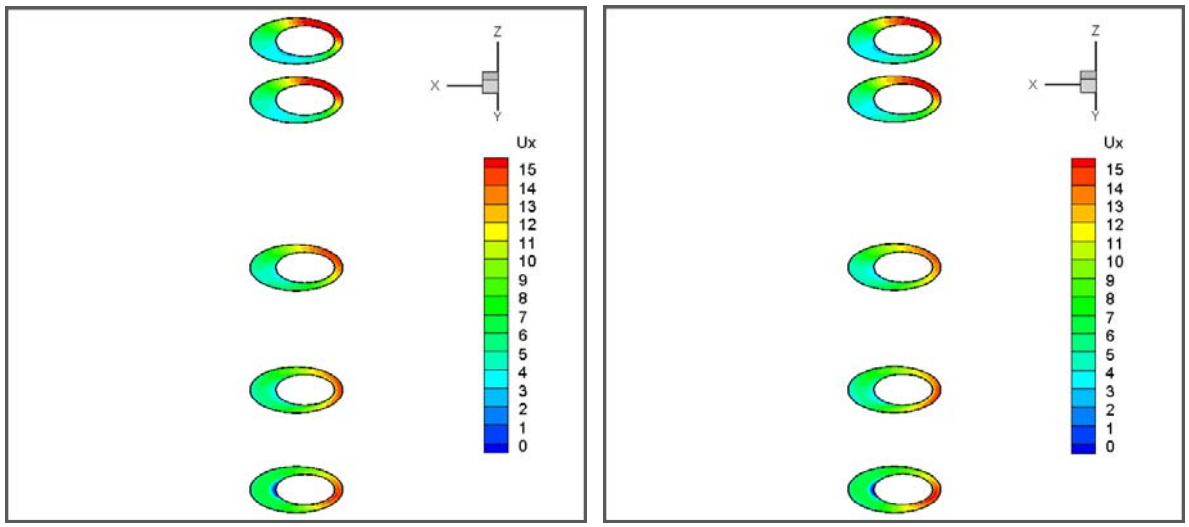

(a) UDF (b) MRF

Fig. 14- contours of Ux at Z/L = 0, 0.22, 0.49, 0.86, 0.99. Seal whirl and spin in counterclockwise direction, clearances have been exagerrated for clarity.

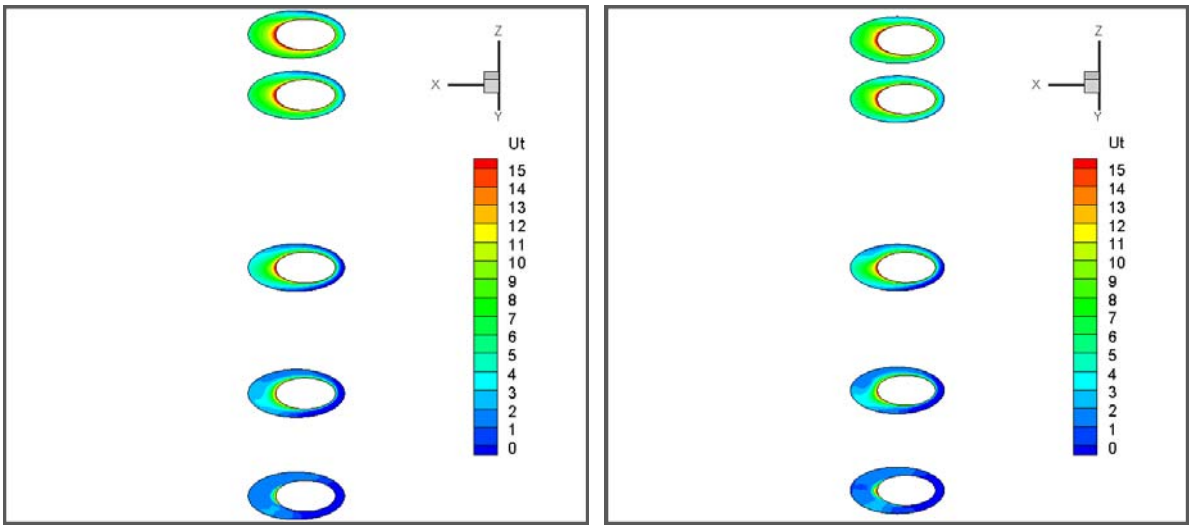

(a) UDF (b) MRF

Fig. 15- contours of Ut at Z/L = 0, 0.22, 0.49, 0.86, 0.99. Seal whirl and spin in counterclockwise direction, clearances have been exagerrated for clarity.

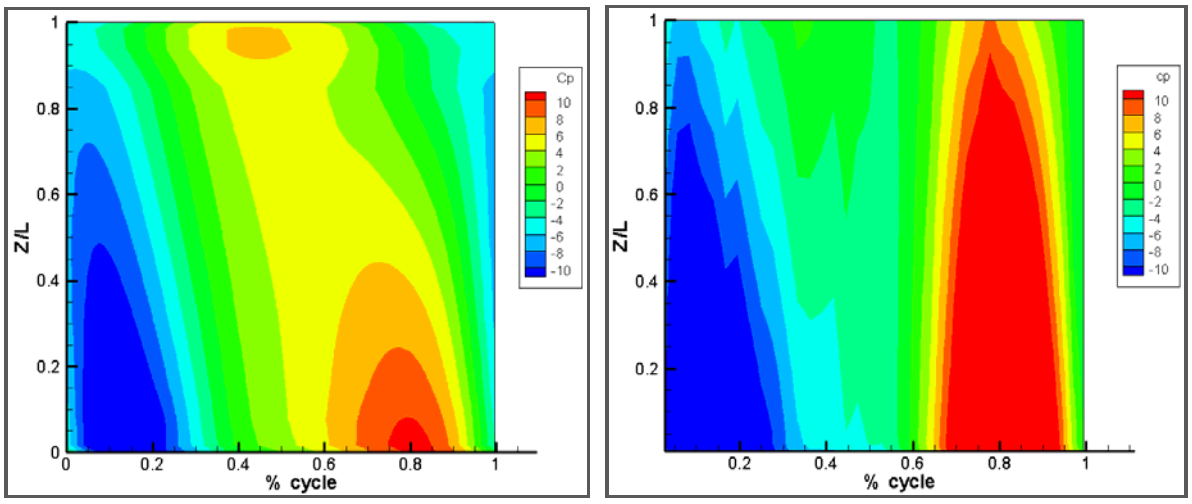

(a) Coordinate transform (ε =50%, β=1) (b) UDF mesh motion (ε =50%, β=1)

Fig. 16- Contours of Coefficent pressure for coordinate transform case and UDF mesh motion case

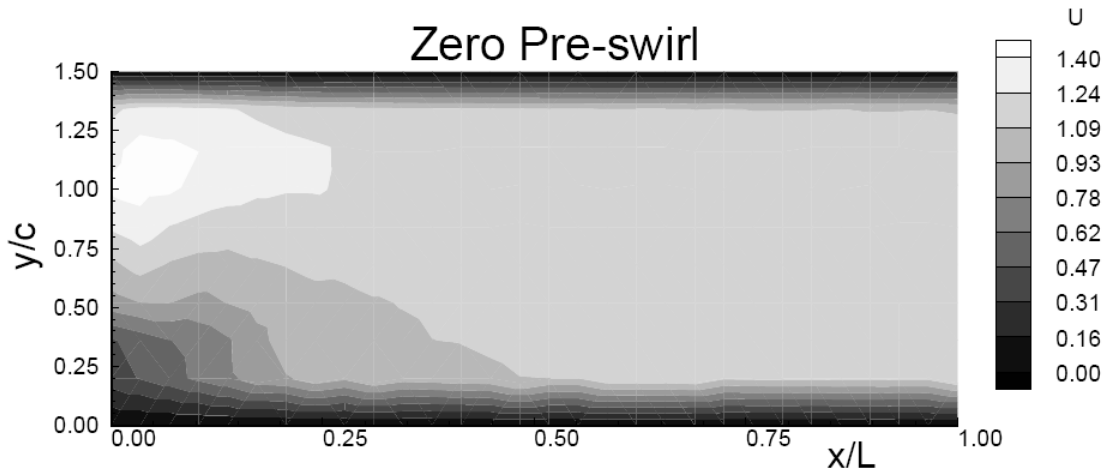

(a) LDV(experimental, from ref. 7)

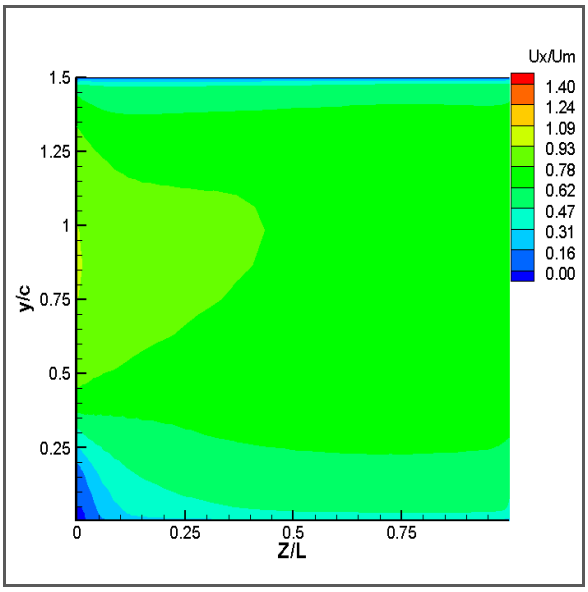

(b)UDF mesh motion

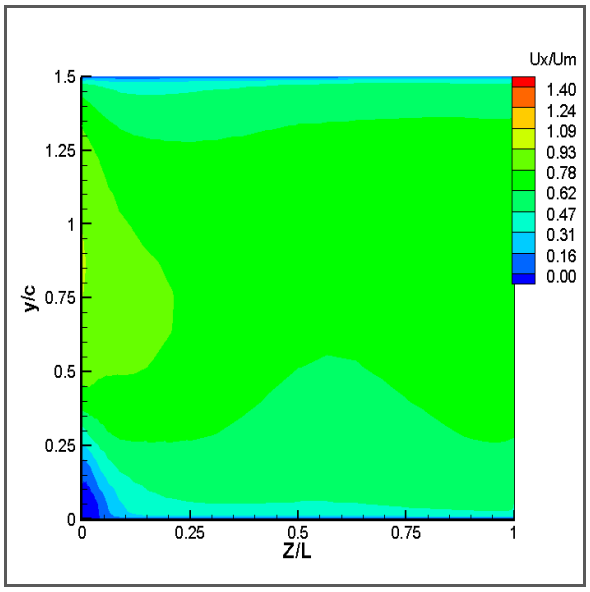

(c)Coordinate Transform

Fig. 17- Contours of axial velocity for Maximum clearance position

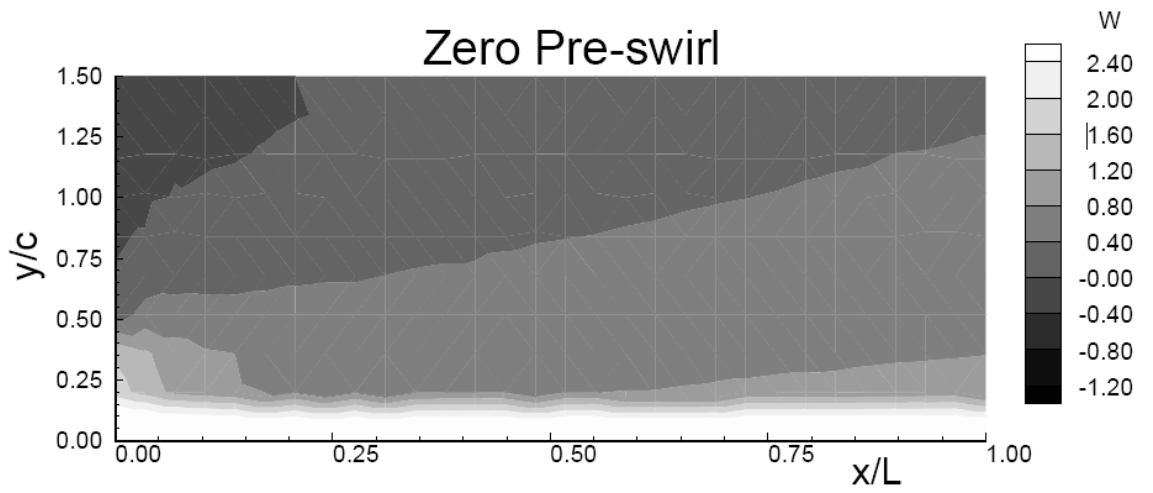

(a) LDV(experimental, from ref. 7)

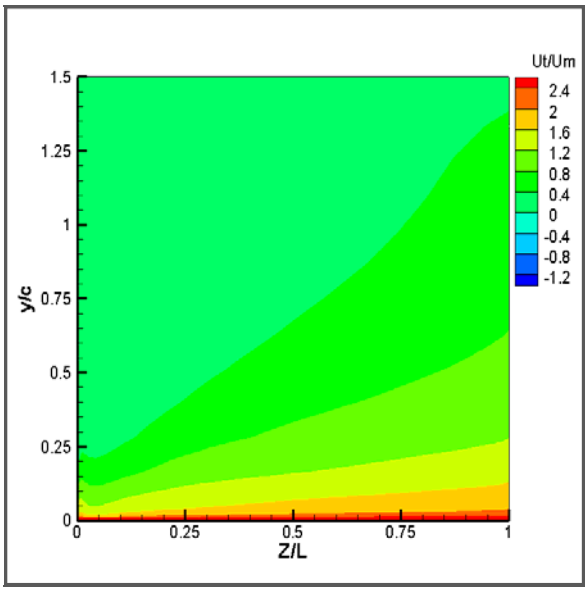

(b)UDF mesh motion

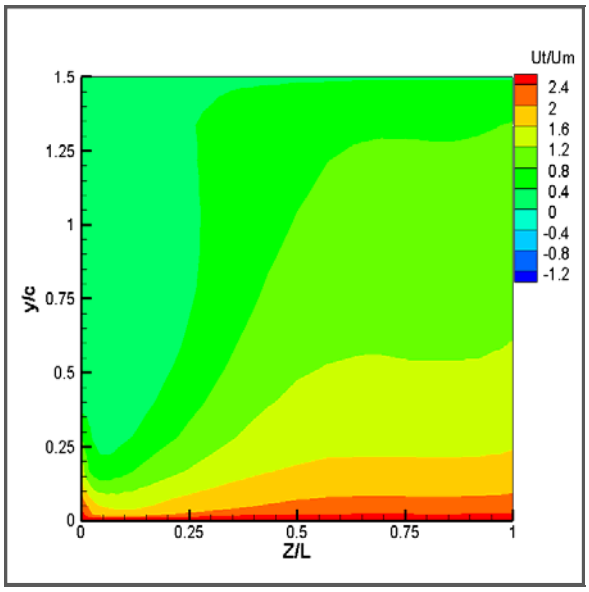

(c)Coordinate Transform

Fig. 18- Contours of tangential velocity for Maximum clearance position

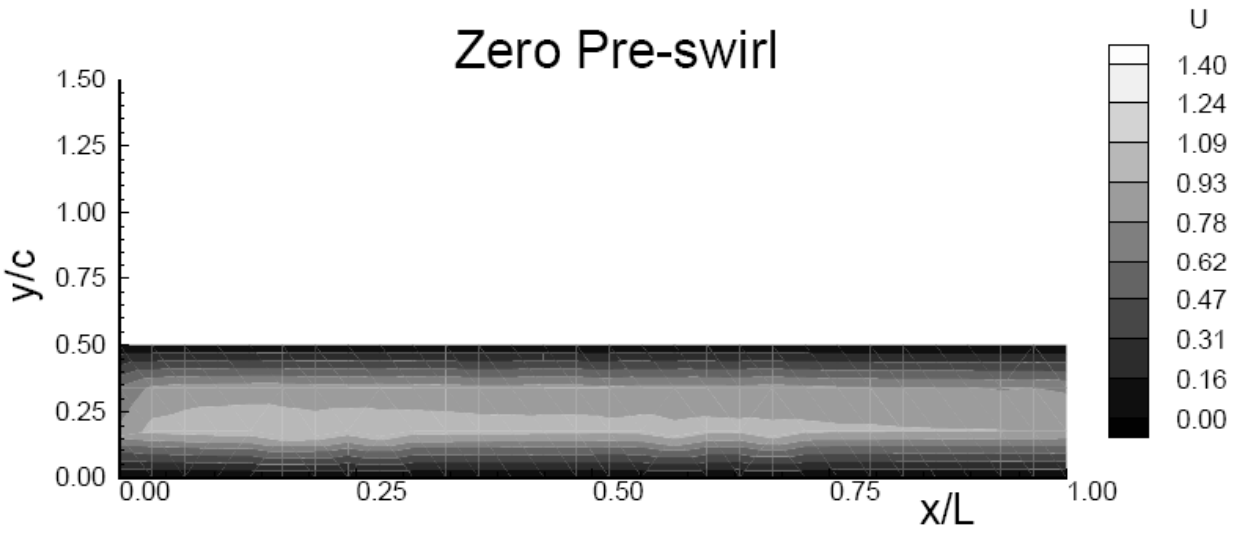

(a) LDV(experimental, from ref. 7)

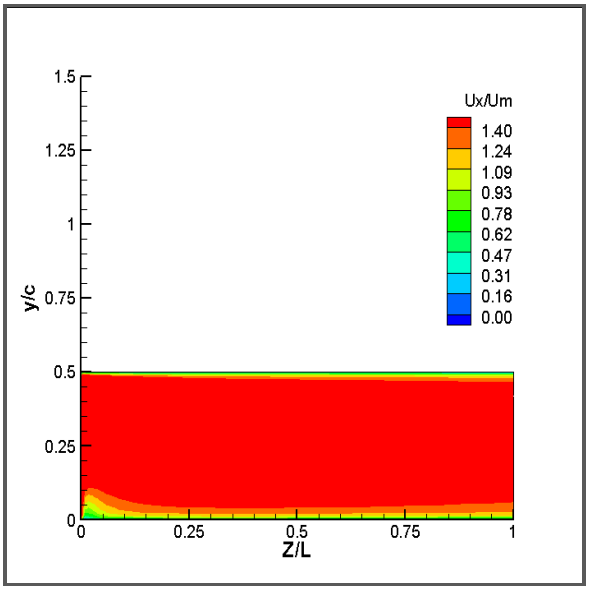

(b)UDF mesh motion

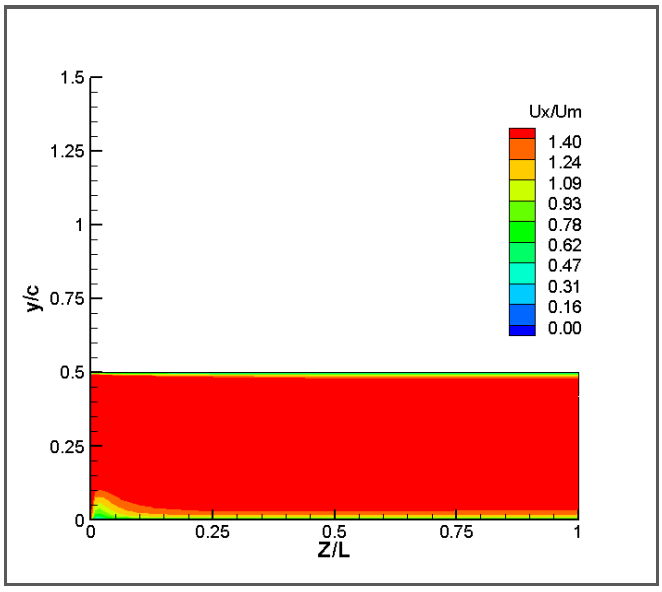

(c)Coordinate Transform

Fig. 19- Contours of axial velocity for Minimum clearance position

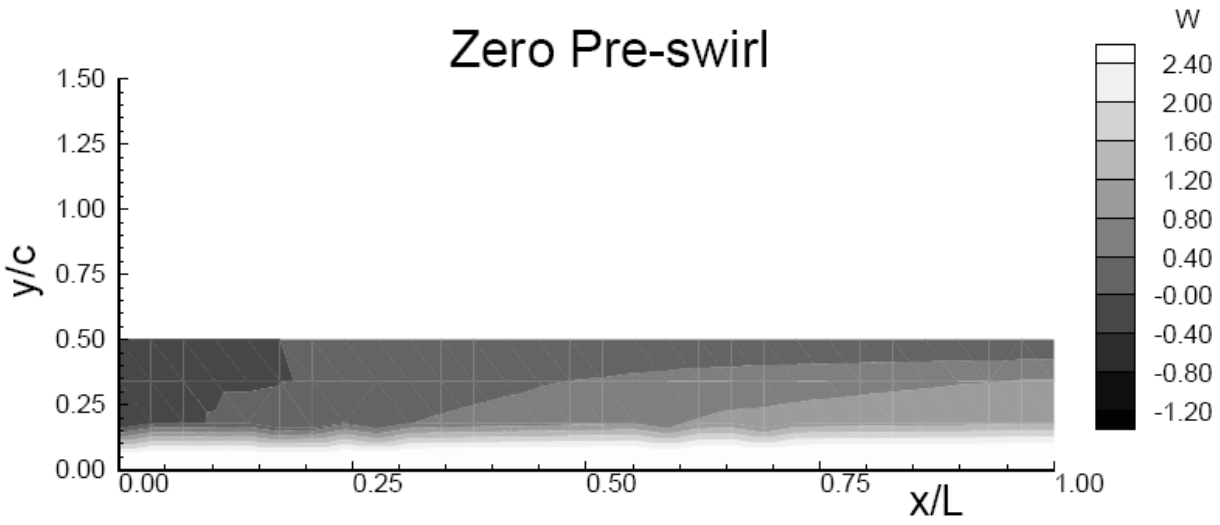

(a) LDV(experimental, from ref. 7)

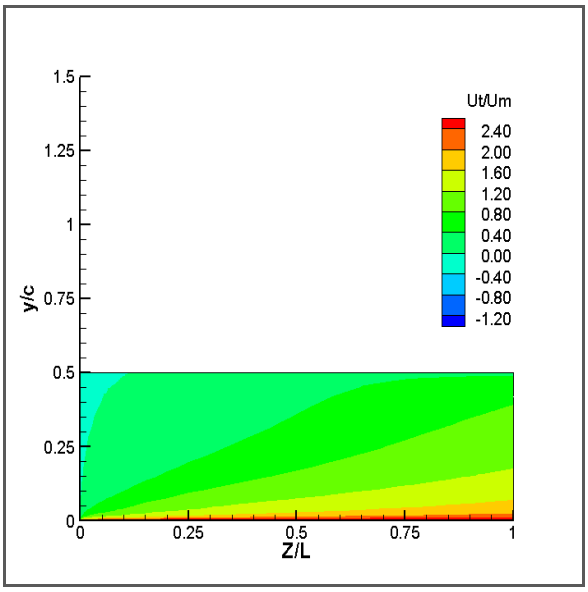

(b)UDF mesh motion

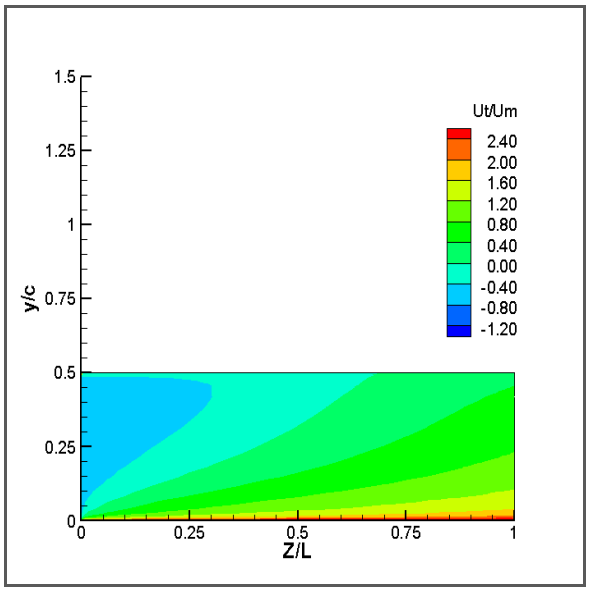

(c)Coordinate Transform

Fig. 20- Contours of tangential velocity for Minimum clearance position

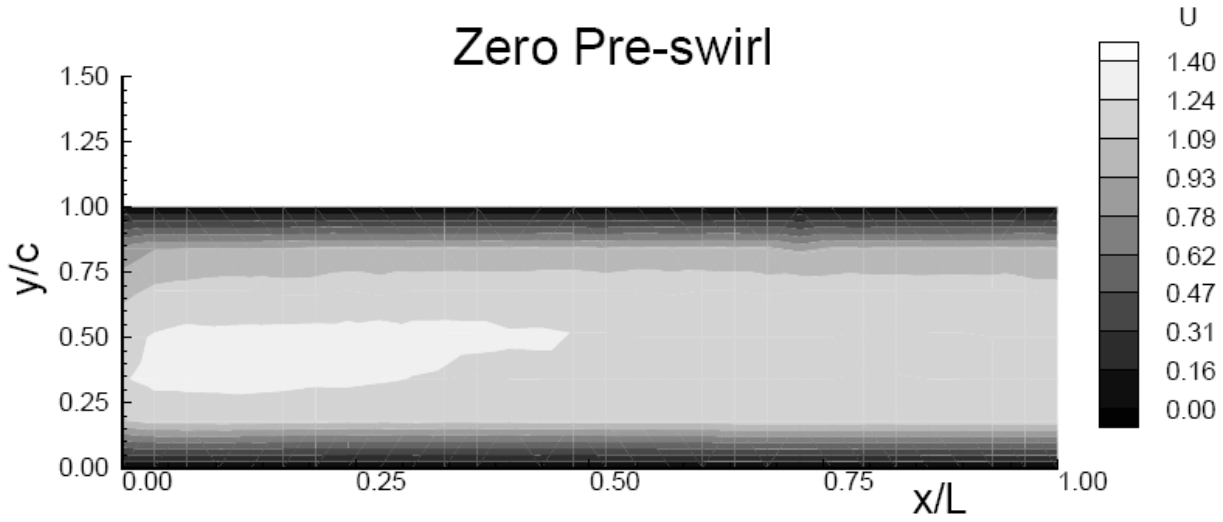

(a) LDV(experimental, from ref. 7)

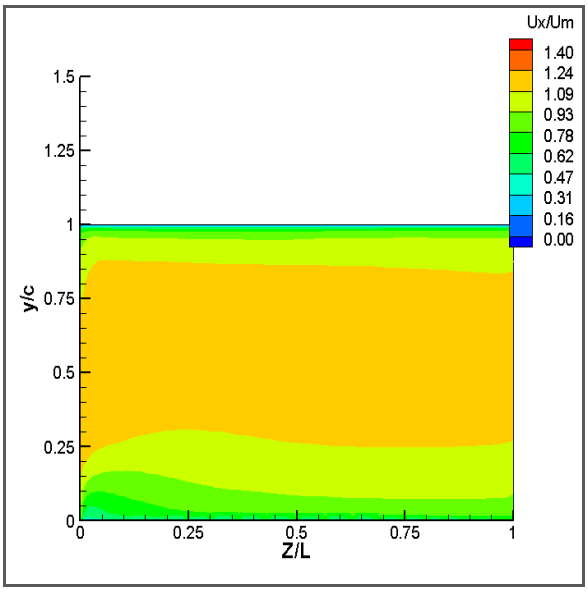

(b)UDF mesh motion

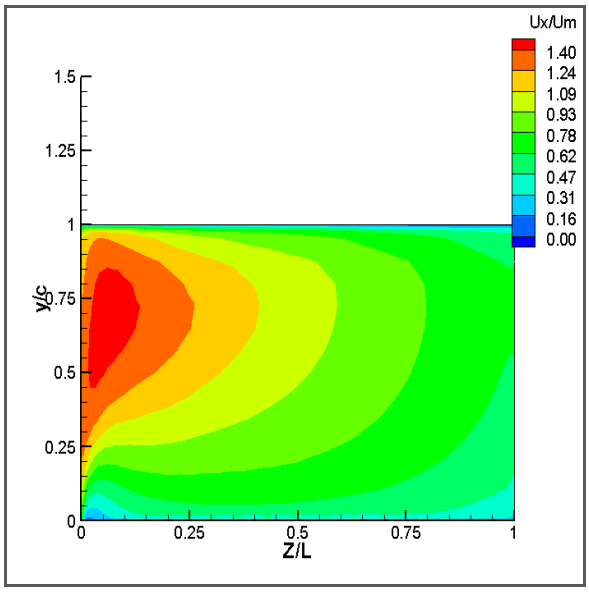

(c)Coordinate Transform

Fig. 21- Contours of axial velocity for Pressure side

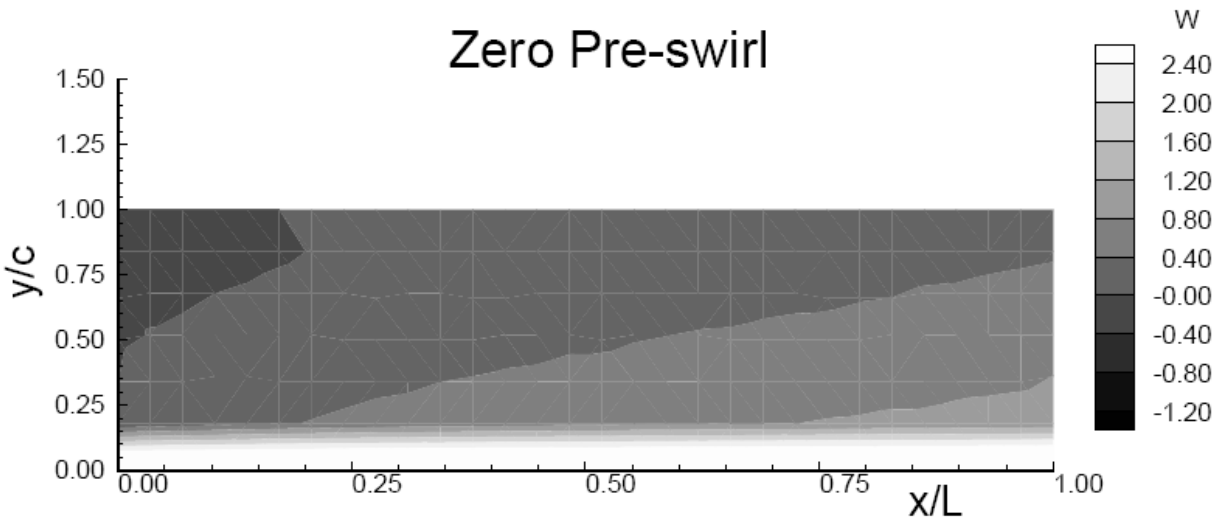

LDV(experimental, from ref. 7)

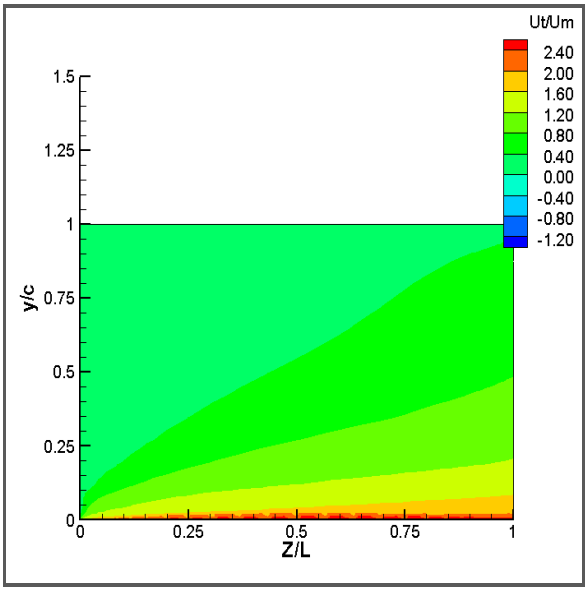

(b)UDF mesh motion

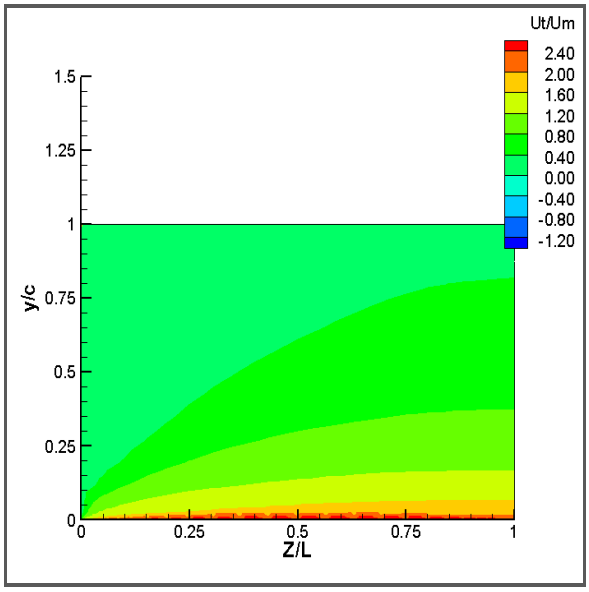

(c)Coordinate Transform

Fig. 22- Contours of tangential velocity for Pressure side

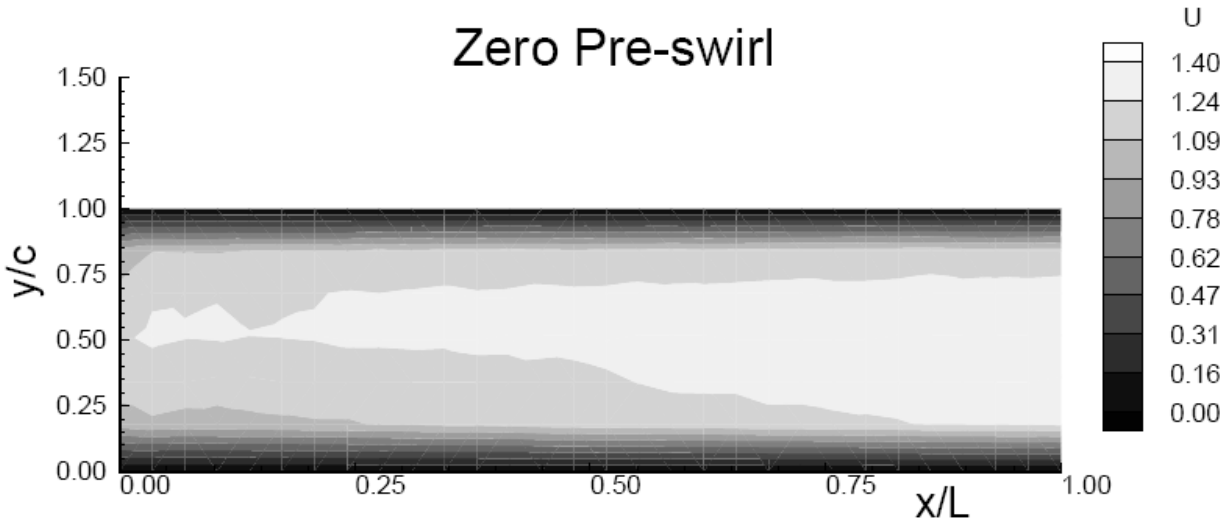

(a) LDV(experimental, from ref. 7)

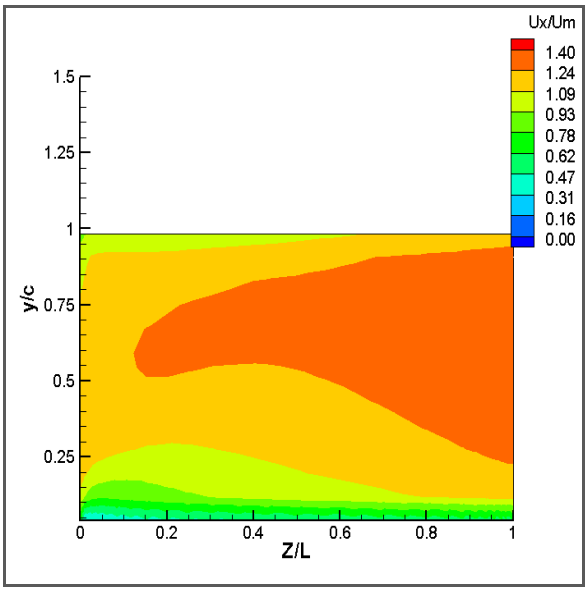

(b)UDF mesh motion

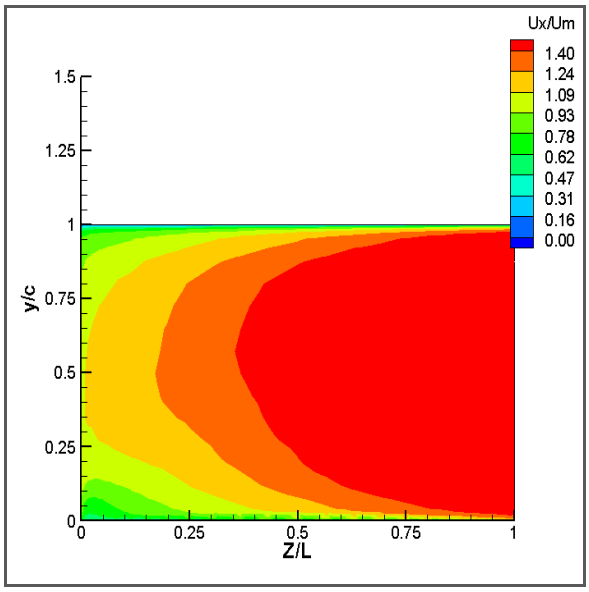

(c)Coordinate Transform

Fig. 23- Contours of axial velocity for Suction side

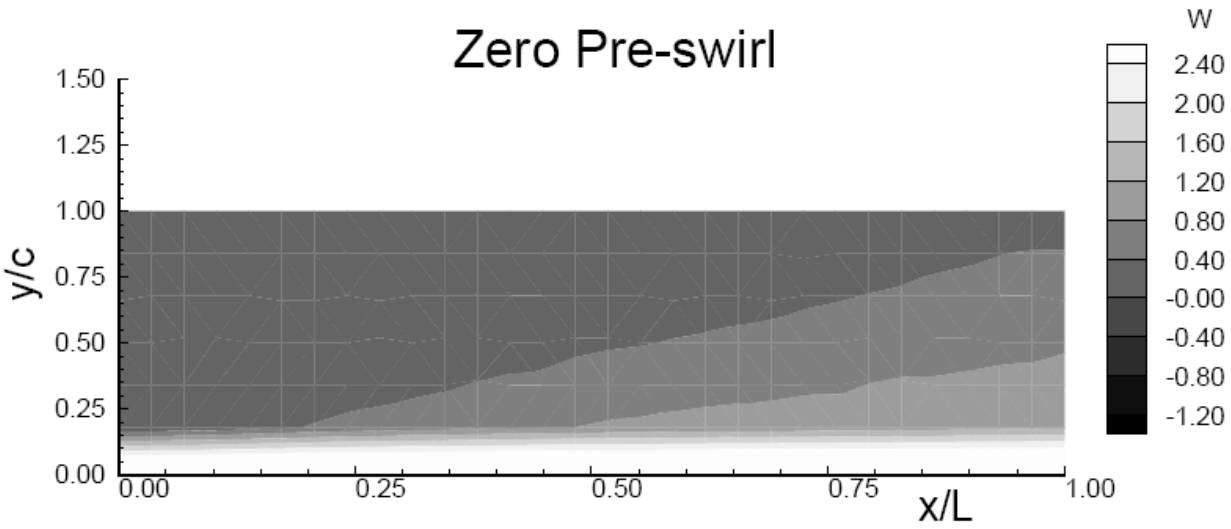

(a) LDV(experimental, from ref. 7)

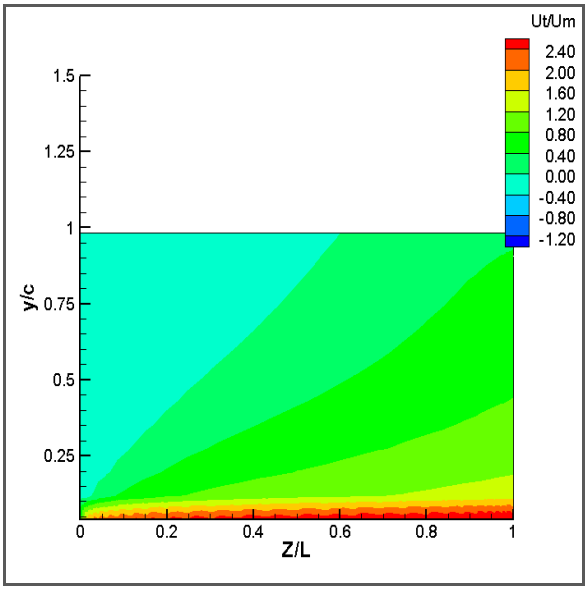

(b)UDF mesh motion

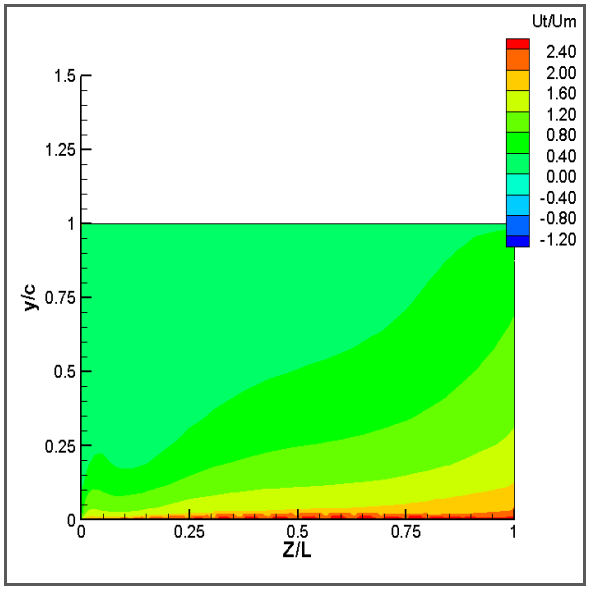

(c)Coordinate Transform

Fig. 24- Contours of axial velocity for Suction side

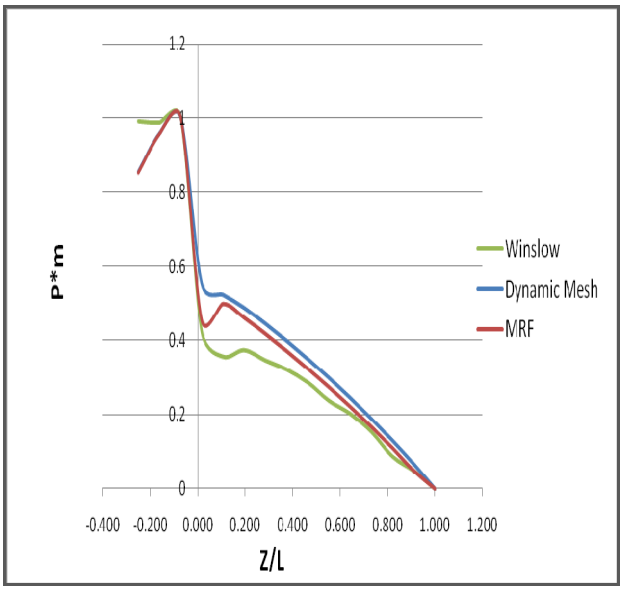

(a)

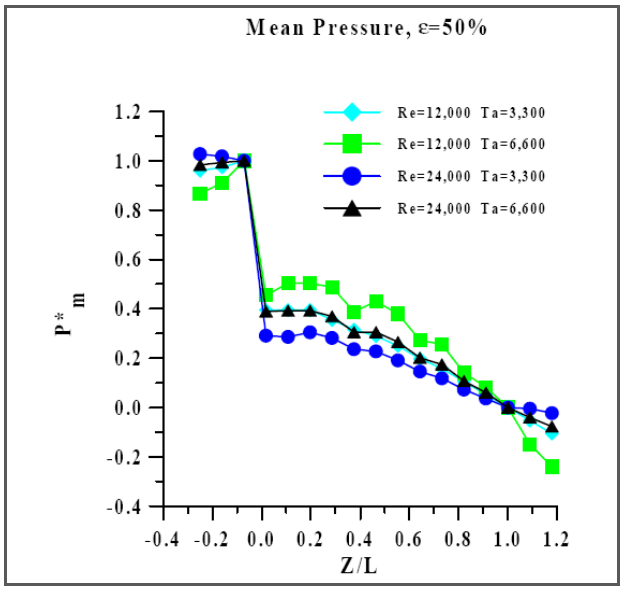

(b) Winslow (1994), Experimental

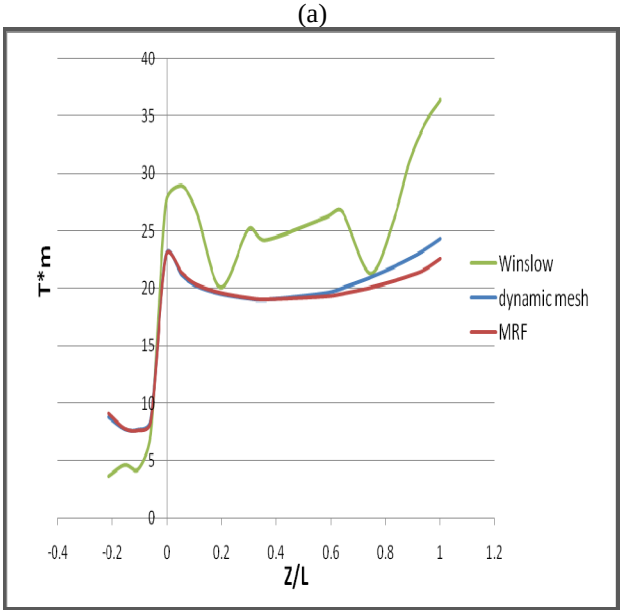

(c)

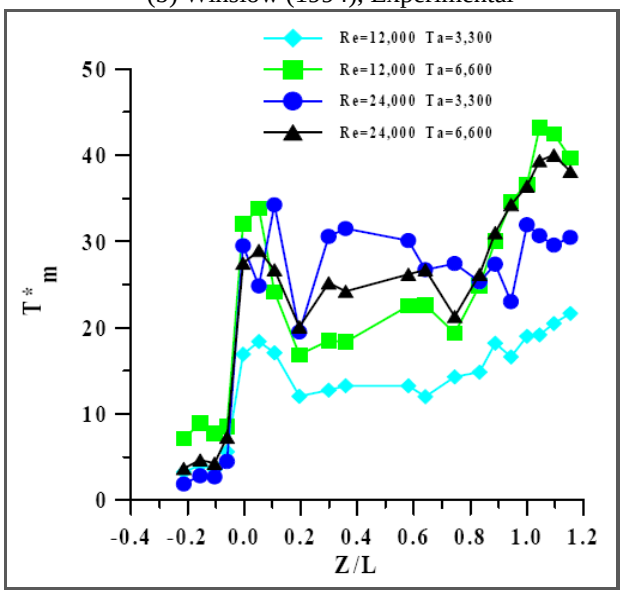

(d) Winslow (1994), Experimental

Fig. 25- Plots of P*m Vs Z/L and T*m Vs Z/L

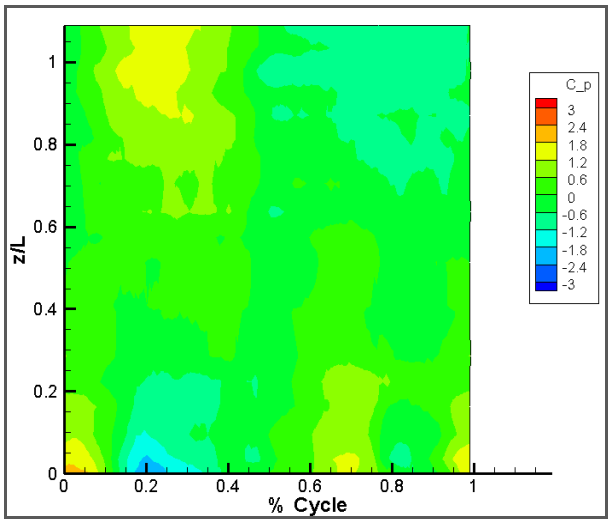

(a) β= 0.3(experimental, from ref. 3)

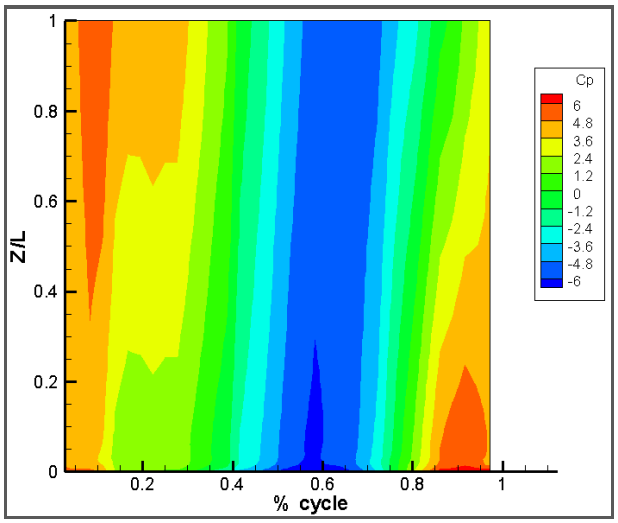

(b) β= 0.3

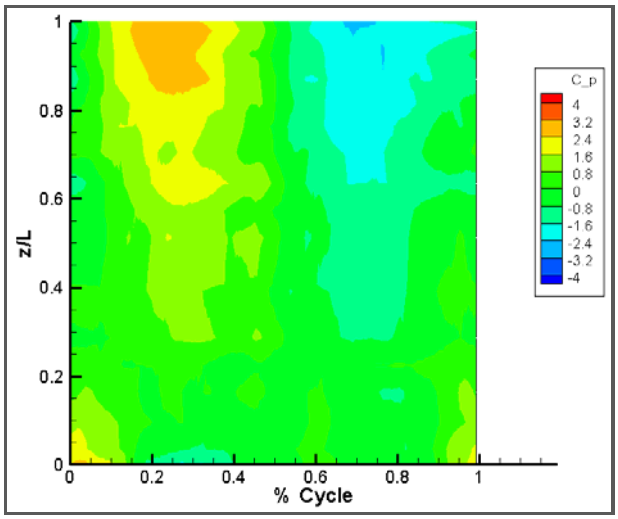

(c) β= 0.4(experimental, from ref. 3)

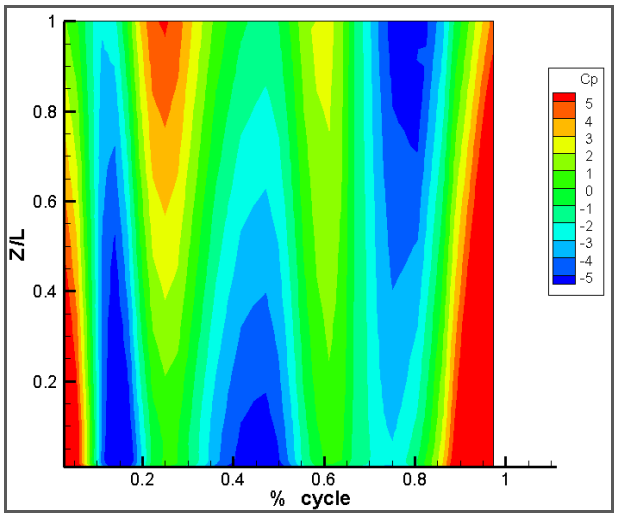

(d) β= 0.4

Fig. 26- Phase Averaged Pressure (Cp), Re=24000, ε =50%, Ta=6600

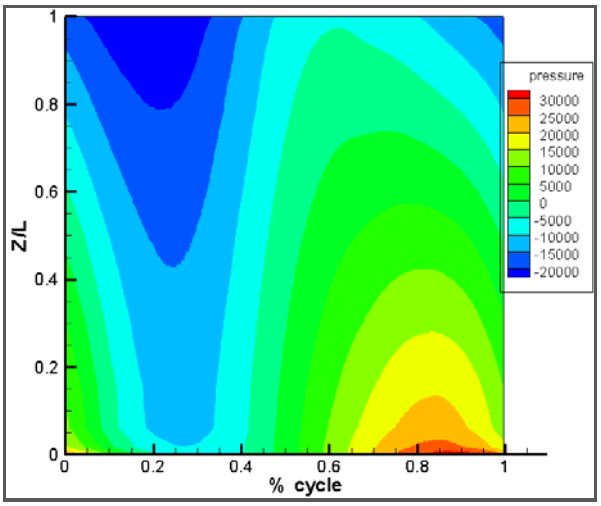

(a) Coordinate Transform (ε =15mil)

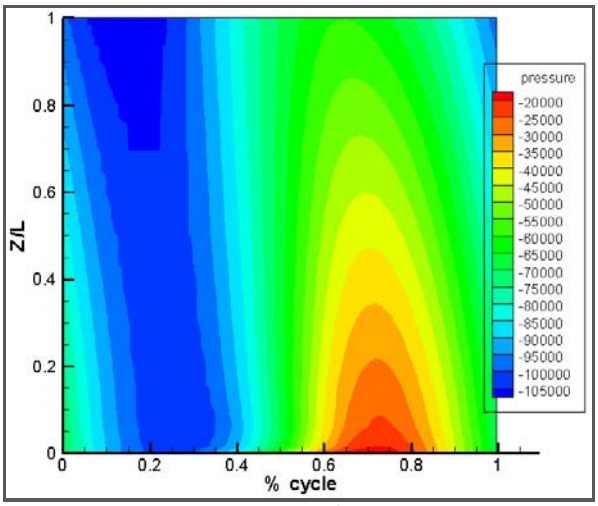

(b) UDF mesh motion-254° Whirl (ε =15mil)

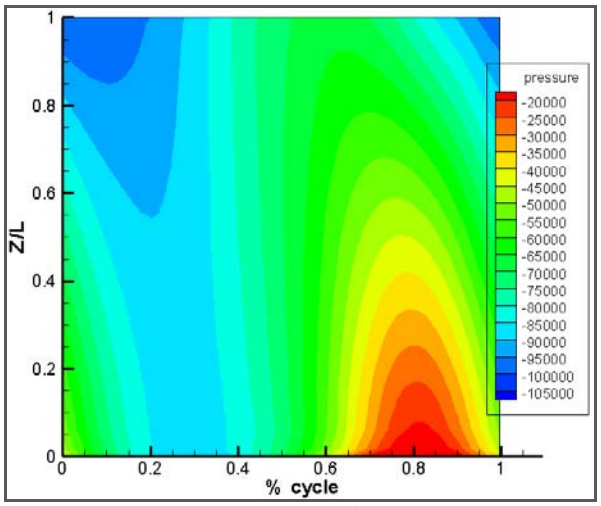

(c) UDF mesh motion-219° Whirl (ε =15mil)

Fig. 27- Contours of static pressure as a function of Z/L and % cycle for ε = 15 mil and β=0.3

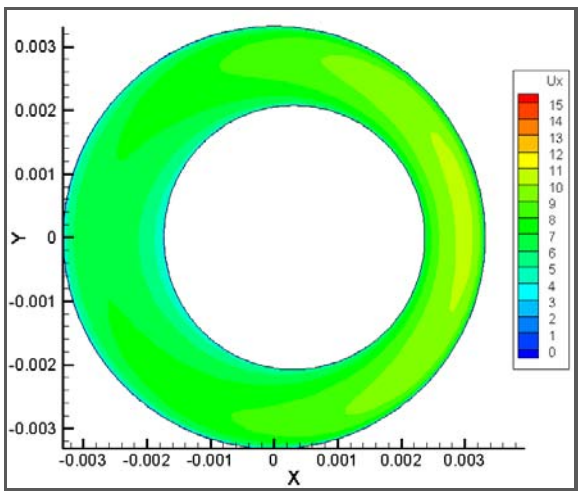

(a) Coordinate Transform (ε=15 mil)

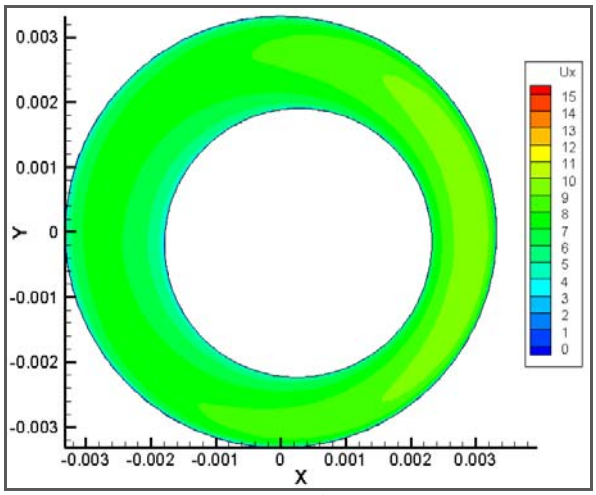

(b) UDF mesh motion-254^{o} Whirl (ε =15mil)

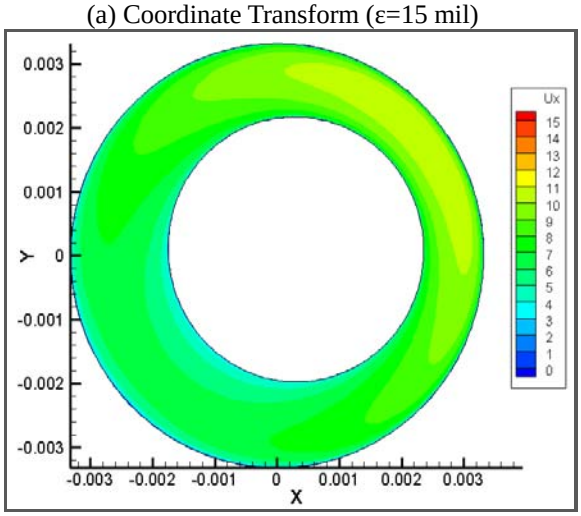

(c) UDF mesh motion-219^{o} Whirl (ε =15mil)

Fig. 28- Contours of axial velocity at Z= 15mm,ε =15mil and β=0.3

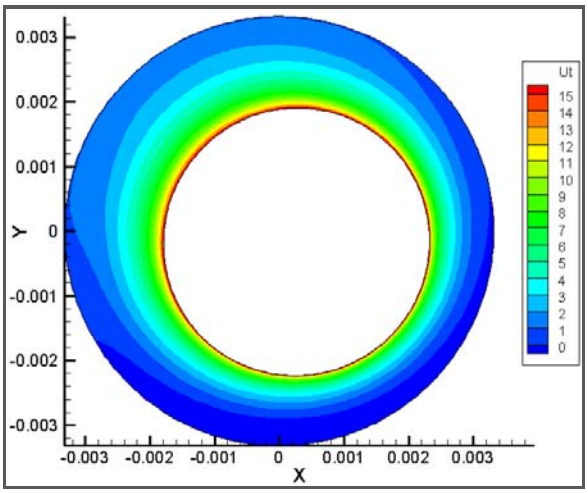

(a) Coordinate Transform (ε=15 mil)

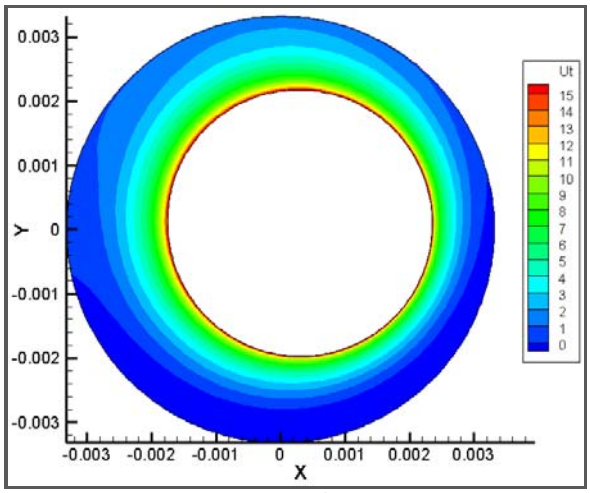

(b)UDF mesh motion-254^{o} Whirl (ε =15mil)

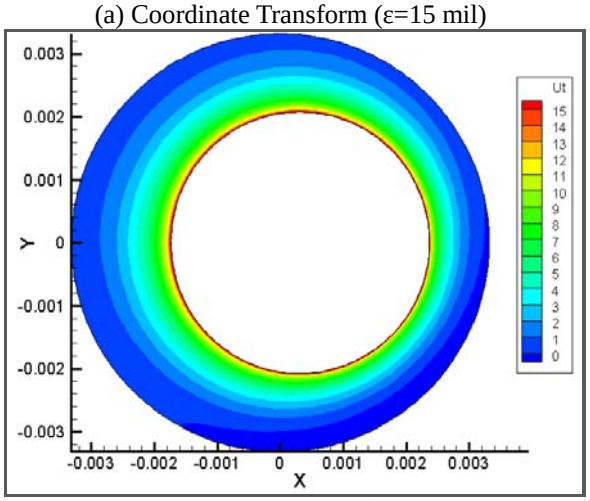

(b)UDF mesh motion-219^{o} Whirl (ε =15mil)

Fig. 29- Contours of tangential velocity at Z= 15mm,ε =15mil and β=0.3